PHYSICAL REVIEW D **90,** 115018 (2014)

Bounds on the mass of doubly charged Higgs bosons in the same-sign diboson decay scenario

Shinya Kanemura,[1,*] Mariko Kikuchi,[1,†] Kei Yagyu,[2,‡] and Hiroshi Yokoya[1,§]

[1]*Department of Physics, University of Toyama, 3190 Gofuku, Toyama 930-8555, Japan*
[2]*Department of Physics, National Central University, Chungli 32001, Taiwan*

(Received 25 July 2014; published 24 December 2014)

A direct search for doubly charged Higgs bosons $H^{\pm\pm}$ is one of the most important probes in the Higgs triplet model, which is motivated by generation mechanisms of tiny neutrino masses. There are two major decay modes of $H^{\pm\pm}$, i.e., the same-sign dilepton decay $H^{\pm\pm} \to \ell^{\pm}\ell^{\pm}$ and the same-sign diboson decay $H^{\pm\pm} \to W^{\pm(*)}W^{\pm(*)}$. For the case where the former decay mode is dominant, the lower limit on the mass of $H^{\pm\pm}$ has been set at about 400 GeV by the ATLAS and CMS Collaborations. On the other hand, for the case where the latter decay mode is dominant, no dedicated search has been performed in the past. By taking into account characteristic signals of $H^{\pm\pm}$ in the diboson decay scenario at LEP and the LHC experiments, we find that the lower mass bound of 60–68 GeV can be obtained by using the same-sign dilepton search performed by the ATLAS Collaboration with 4.7 fb^{-1} data at the collision energy of 7 TeV. We also show that the limit can be extended up to about 85–90 GeV, assuming the integrated luminosity of 20 fb^{-1} and 7 TeV for the collision energy. We give detailed explanations on the decay properties of $H^{\pm\pm}$ for relatively small mass cases and also on production cross sections of $H^{\pm\pm}$ at the next-to-leading order of QCD at the LHC.

DOI: 10.1103/PhysRevD.90.115018 PACS numbers: 12.60.Fr, 14.80.Fd

I. INTRODUCTION

In 2012, a Higgs boson was discovered at the CERN Large Hadron Collider (LHC) [1,2]. Its observed properties are consistent with the prediction in the standard model (SM) within the current experimental uncertainties [3]. In addition, so far, no report has been delivered to us for the discovery of other new particles. Therefore, it has been found that the SM is a good description for particle physics at the scale of hundreds of GeV, not only in the gauge interactions but also in the sector of electroweak symmetry breaking.

Although the Higgs boson has been discovered and its property has turned out to be SM-like, we know nothing about the structure of the Higgs sector. In fact, the minimal Higgs sector with one isospin doublet scalar field is just an assumption without any theoretical principle. Thus, it is natural to consider a possibility that the Higgs sector takes a nonminimal form with additional isospin multiplet scalar fields, such as an extra singlet, doublet, triplet, and so on. Most of these nonminimal Higgs sectors can explain current experimental data as well. Furthermore, these extended Higgs sectors are often introduced in the context of new physics models which try to explain the phenomena beyond the SM, i.e., neutrino masses, dark matter, and baryogenesis. Therefore, it is very important to experimentally explore the possibility of extended Higgs sectors. We then may be able to discriminate new physics models from the property of the Higgs sector.

For example, extended Higgs sectors with multidoublet scalar fields are introduced in supersymmetric extensions of the SM. They are also motivated to introduce an additional source of CP violation [4] and to realize the strong first-order phase transition [5], both of which are required to have successful electroweak baryogenesis [6]. Singlet scalar fields are often introduced in models with the spontaneously broken $B - L$ gauge symmetry [7]. The Higgs sector with a complex triplet scalar field appears in models that can explain neutrino masses via the seesaw mechanism [8]. Tiny neutrino masses can also be explained via the loop-induced effects of extended scalar sectors [9–12]. Extended scalar sectors with a discrete symmetry such as Z_2 can provide a candidate for dark matter [13,14].

We here focus on the Higgs triplet model (HTM) [8]. Its Higgs sector is composed of an isospin doublet Higgs field with a hypercharge[1] $Y = 1/2$ and an isospin triplet Higgs field with $Y = 1$. In this model, Majorana masses of neutrinos are generated via new Yukawa interactions among the left-handed lepton doublets and the Higgs triplet field; $(m_\nu)_{ij} \propto h_{ij} v_\Delta$, where v_Δ is the vacuum expectation value (VEV) of the triplet field and h_{ij} is a matrix in the Lagrangian for the Yukawa interactions.

*kanemu@sci.u-toyama.ac.jp
†kikuchi@jodo.sci.u-toyama.ac.jp
‡keiyagyu@ncu.edu.tw
§hyokoya@sci.u-toyama.ac.jp

[1]We adopt the notation of Y as $Q = T^3 + Y$, where Q is the electric charge and T^3 is the third component of the isospin.

One of the most characteristic features of the HTM is the existence of doubly charged Higgs bosons $H^{\pm\pm}$, in addition to the other additional Higgs bosons, i.e., singly charged $H^{\pm}$, CP-even H, and CP-odd A Higgs bosons. The discovery of $H^{\pm\pm}$ at collider experiments is the direct evidence of the HTM. Production of these bosons at collider experiments has been studied in Refs. [15–36]. For the decay of $H^{\pm\pm}$, there are three sources, i.e., the Yukawa interactions with left-handed lepton doublets, electroweak gauge interactions of the gauge-gauge-scalar type, and those of the gauge-scalar-scalar type. They cause the same-sign dilepton decay $H^{\pm\pm} \to \ell^{\pm}\ell^{\pm}$, the same-sign diboson decay $H^{\pm\pm} \to W^{\pm}W^{\pm}$, and the cascade decay $H^{\pm\pm} \to H^{\pm}W^{\pm}$, respectively.[2]

Although the dominant decay mode of $H^{\pm\pm}$ is determined by parameters in the model, the dilepton decay scenario has been considered as the most promising one for discovery [15,17,20,22,23,25,32], because of its cleanness for the detection at colliders. It is also quite appealing that the structure of the neutrino mass matrix can be directly tested by measuring the dileptonic branching ratios of $H^{\pm\pm}$ [17,20,22] and $H^{\pm}$ [22,38], because the branching ratios are predominantly determined by the neutrino Yukawa couplings. In this scenario, a sharp peak in the invariant mass distribution of the same-sign dilepton is the characteristic signal of $H^{\pm\pm}$. The experimental searches for $H^{\pm\pm}$ in the same-sign dilepton events have been performed at LEP [39], HERA [40], Tevatron [41,42], and the LHC [43,44]. Assuming that the branching ratio of $H^{\pm\pm}$ decay into $\mu^{\pm}\mu^{\pm}$ is 100%, the strongest lower bound on the mass of doubly charged Higgs bosons has been obtained as 459 GeV at the LHC [44]. Current bounds have also been set at around 400 GeV in several benchmark points for the structure of the neutrino mass matrix [44].

In this paper, we discuss the direct searches for $H^{\pm\pm}$ in the diboson decay scenario, where $H^{\pm\pm}$ predominantly decay into same-sign W bosons, at the past, current, and future collider experiments, such as LEP and the LHC with the 7–8 TeV and 13–14 TeV runs. The same-sign diboson decay scenario is equally important to the same-sign dilepton decay scenario in the HTM. Collider phenomenology for this decay mode has been studied in Refs. [21,30,33,36]. In Ref. [33], the lower limit on the mass of $H^{\pm\pm}$ has been derived by using the same-sign dilepton events collected by the ATLAS Collaboration at the LHC with 7 TeV and 4.7 fb^{-1} data [45]. To our knowledge, this is the first analysis for the constraints on $H^{\pm\pm}$ in the diboson scenario. The aim of the present paper is to explain details of the analysis done in Ref. [33] and to make an update on the results by including the QCD correction to the production cross sections.

This paper is organized as follows. In Sec. II, we briefly review the HTM. After we define the mass eigenstates for the Higgs bosons, we derive the Yukawa interaction and the gauge interaction for the tripletlike Higgs bosons at tree level. In Sec. III, we give expressions for the decay rates of $H^{\pm\pm}$ in all three decay modes. Partial decay widths of $H^{\pm\pm}$ are evaluated with particular attention to the case of relatively small masses where one or both of the W bosons are forced off shell. We then show the phase diagram indicating the main decay mode of $H^{\pm\pm}$. Next, we evaluate the cross section of $H^{\pm\pm}$ productions at the LHC in the leading order (LO) and the next-to-leading order (NLO) of QCD. In Sec. IV, we exhibit constraints on the mass of $H^{\pm\pm}$ in the diboson decay scenario at the LEP experiments and also at the LHC. At the LEP I experiment, the lower limit on the mass of $H^{\pm\pm}$ can be obtained from the total width of the Z boson. We also evaluate the expected number of events for the various final states in the process of $e^+e^- \to H^{++}H^{--}$ at the LEP II experiment. We then discuss the mass bound on $H^{\pm\pm}$ by using the current LHC limit on the cross section for anomalous production of same-sign dileptons. Section V is devoted to our conclusion. In the Appendix, the cross sections for $H^{\pm\pm}$ production at the LHC with various collision energies are collected for the reader's convenience.

II. THE HIGGS TRIPLET MODEL

The scalar sector of the HTM is composed of the isospin doublet field Φ with hypercharge $Y = 1/2$ and the triplet field Δ with $Y = 1$. The most general form of the Higgs potential under the gauge symmetry is written as

$$\begin{aligned} V(\Phi,\Delta) = {} & m^2\Phi^\dagger\Phi + M^2\mathrm{Tr}(\Delta^\dagger\Delta) + [\mu\Phi^T i\tau_2\Delta^\dagger\Phi + \mathrm{H.c.}] \\ & + \lambda_1(\Phi^\dagger\Phi)^2 + \lambda_2[\mathrm{Tr}(\Delta^\dagger\Delta)]^2 + \lambda_3\mathrm{Tr}[(\Delta^\dagger\Delta)^2] \\ & + \lambda_4(\Phi^\dagger\Phi)\mathrm{Tr}(\Delta^\dagger\Delta) + \lambda_5\Phi^\dagger\Delta\Delta^\dagger\Phi, \end{aligned} \tag{1}$$

where all the parameters are taken to be real without loss of generality [46]. The Higgs fields can be parameterized as

$$\Phi = \begin{pmatrix} \phi^+ \\ \phi^0 \end{pmatrix}, \qquad \Delta = \begin{pmatrix} \frac{\Delta^+}{\sqrt{2}} & \Delta^{++} \\ \Delta^0 & -\frac{\Delta^+}{\sqrt{2}} \end{pmatrix}, \tag{2}$$

where the neutral components are expressed as

$$\begin{aligned} \phi^0 &= \frac{1}{\sqrt{2}}(\phi_R^0 + v_\phi + i\phi_I^0), \\ \Delta^0 &= \frac{1}{\sqrt{2}}(\Delta_R^0 + v_\Delta + i\Delta_I^0). \end{aligned} \tag{3}$$

[2]In principle, $H^{\pm\pm} \to H^{\pm}H^{\pm}$ decay occurs via the scalar triple couplings, if there is a large mass difference between $H^{\pm\pm}$ and $H^{\pm}$. However, such a situation is severely constrained by electroweak precision measurements [37].

The VEVs of the doublet and triplet Higgs fields are denoted by v_ϕ and v_Δ, respectively. They are related to the Fermi constant G_F by $v^2 \equiv v_\phi^2 + 2v_\Delta^2 = (\sqrt{2}G_F)^{-1}$. The nonzero v_Δ deviates the electroweak rho parameter from unity at tree level:

$$\rho \equiv \frac{m_W^2}{m_Z^2 \cos^2\theta_W} = \frac{1+\frac{2v_\Delta^2}{v_\phi^2}}{1+\frac{4v_\Delta^2}{v_\phi^2}}, \tag{4}$$

where m_W, m_Z, and θ_W are the W boson mass, the Z boson mass, and the weak mixing angle, respectively. Since the experimental value of the rho parameter is close to unity, i.e., $\rho_{\rm exp} = 1.0004^{+0.0003}_{-0.0004}$ [47], v_Δ has to be less than about 3.5 GeV at the 95% confidence level (C.L.).

Mass eigenstates in the doubly charged states ($H^{\pm\pm}$) purely come from Δ; i.e., $H^{\pm\pm} = \Delta^{\pm\pm}$. For the other scalar bosons, mass eigenstates are defined by introducing the following orthogonal transformations:

$$\begin{aligned}
\begin{pmatrix}\phi_R^0\\ \Delta_R^0\end{pmatrix} &= \begin{pmatrix}\cos\alpha & -\sin\alpha\\ \sin\alpha & \cos\alpha\end{pmatrix}\begin{pmatrix}h\\ H\end{pmatrix},\\
\begin{pmatrix}\phi^\pm\\ \Delta^\pm\end{pmatrix} &= \begin{pmatrix}\cos\beta & -\sin\beta\\ \sin\beta & \cos\beta\end{pmatrix}\begin{pmatrix}G^\pm\\ H^\pm\end{pmatrix},\\
\begin{pmatrix}\phi_I^0\\ \Delta_I^0\end{pmatrix} &= \begin{pmatrix}\cos\beta' & -\sin\beta'\\ \sin\beta' & \cos\beta'\end{pmatrix}\begin{pmatrix}G^0\\ A\end{pmatrix},
\end{aligned} \tag{5}$$

where mixing angles α, β, and β' are given, respectively, by

$$\begin{aligned}
\tan 2\alpha &= \frac{v_\Delta}{v_\phi}\frac{2v_\phi^2(\lambda_4+\lambda_5) - 4M_\Delta^2}{2v_\phi^2\lambda_1 - M_\Delta^2 - 2v_\Delta^2(\lambda_2+\lambda_3)},\\
\tan\beta &= \frac{\sqrt{2}v_\Delta}{v_\phi}, \qquad \tan\beta' = \frac{2v_\Delta}{v_\phi},
\end{aligned} \tag{6}$$

with

$$M_\Delta^2 \equiv \frac{v_\phi^2\mu}{\sqrt{2}v_\Delta}. \tag{7}$$

In Eq. (5), $G^\pm$ and G^0 are the Nambu-Goldstone bosons which are absorbed into the longitudinal component of W and Z bosons, respectively. Because all the mixing angles given in Eq. (6) are quite small due to $v_\Delta/v_\phi \ll 1$, $H^\pm$, A, and H are mostly composed of the triplet Higgs field. We thus call these scalars ($H^\pm$, A, H, and $H^{\pm\pm}$) the tripletlike Higgs bosons. On the other hand, by the same reason, h can be regarded as the SM-like Higgs boson, because it mainly comes from the doublet Higgs field. By neglecting $\mathcal{O}(v_\Delta^2)$ terms, the masses of these physical Higgs bosons are given in a good approximation by

$$\begin{aligned}
m_{H^{\pm\pm}}^2 &\simeq M_\Delta^2 - \frac{\lambda_5}{2}v^2, \qquad m_{H^\pm}^2 \simeq M_\Delta^2 - \frac{\lambda_5}{4}v^2,\\
m_A^2 &\simeq m_H^2 \simeq M_\Delta^2,
\end{aligned} \tag{8}$$

$$m_h^2 \simeq 2\lambda_1 v^2. \tag{9}$$

Thus, it can be observed that there are relationships among the masses of tripletlike Higgs bosons [27,28]; i.e., $m_{H^{\pm\pm}}^2 - m_{H^\pm}^2 \simeq m_{H^\pm}^2 - m_A^2$ and $m_A^2 \simeq m_H^2$. From these relations, three patterns of the mass spectrum arise. The first two patterns are $m_A > m_{H^\pm} > m_{H^{\pm\pm}}$ in the case with $\lambda_5 > 0$ and $m_{H^{\pm\pm}} > m_{H^\pm} > m_A$ in the case with $\lambda_5 < 0$. In the special case with $\lambda_5 = 0$, all the tripletlike Higgs bosons degenerate in mass.

The kinetic term of the Lagrangian for the Higgs fields is given by

$$\mathcal{L}_{\rm kin} = |D_\mu\Phi|^2 + {\rm Tr}[(D_\mu\Delta)^\dagger(D^\mu\Delta)], \tag{10}$$

where the covariant derivatives are defined as

$$\begin{aligned}
D_\mu\Phi &= \left(\partial_\mu - i\frac{g}{2}\tau^a W_\mu^a - i\frac{g'}{2}B_\mu\right)\Phi,\\
D_\mu\Delta &= \partial_\mu\Delta - i\frac{g}{2}[\tau^a W_\mu^a, \Delta] - ig'B_\mu\Delta.
\end{aligned} \tag{11}$$

From the above Lagrangian, Higgs-gauge-gauge–type vertices are derived. Coefficients of the vertices for the tripletlike Higgs bosons are given as follows:

$$\begin{aligned}
&(H^{\pm\pm}W_\mu^\mp W_\nu^\mp): \ -gm_W\sin\beta g_{\mu\nu},\\
&(H^\pm W_\mu^\mp Z_\nu): \ -\frac{g}{\cos\theta_W}m_W\sin\beta\cos\beta g_{\mu\nu},\\
&(HW_\mu^\pm W_\nu^\mp): \ -gm_W(\cos\beta\sin\alpha - \sqrt{2}\sin\beta\cos\alpha)g_{\mu\nu},\\
&(HZ_\mu Z_\nu): \ -\frac{g}{\cos\theta_W}m_Z(\cos\beta'\sin\alpha - 2\sin\beta'\cos\alpha)g_{\mu\nu}.
\end{aligned} \tag{12}$$

We note that, according to Eq. (6), all the couplings are proportional to v_Δ/v.

Next, we introduce the Yukawa interaction terms with the triplet field. Left-handed lepton doublet fields L_L can couple to the triplet Higgs field by

$$\mathcal{L}_Y = h_{ij}\overline{L_L^{ic}}i\tau_2\Delta L_L^j + {\rm H.c.} \tag{13}$$

If we extract the VEV in the neutral component of the triplet field, we find a Majorana mass term for neutrinos [8]:

$$(m_\nu)_{ij} = \sqrt{2}h_{ij}v_\Delta. \tag{14}$$

From Eq. (14), the magnitudes of h_{ij} are determined by v_Δ, because the value of the left-hand side of the equation is given by the neutrino data. As seen in the text below Eq. (4), v_Δ is limited to at most ~3.5 GeV by the data of electroweak precision observables. Couplings of the

Yukawa interactions among the tripletlike Higgs bosons and leptons are expressed in terms of v_Δ and the neutrino mass matrix $(m_\nu)_{ij}$ with the use of Eq. (14) as follows:

$$(H^{++}\ell_i^-\ell_j^-)\colon -\frac{(m_\nu)_{ij}}{\sqrt{2}v_\Delta}P_L,\quad (H^+\ell_i^-\nu_j)\colon -\frac{(m_\nu)_{ij}}{v_\Delta}\cos\beta P_L,$$
$$(H\nu_i\nu_j)\colon \frac{(m_\nu)_{ij}}{2v_\Delta}\cos\alpha P_L,\quad (A\nu_i\nu_j)\colon i\frac{(m_\nu)_{ij}}{2v_\Delta}\cos\beta' P_L, \tag{15}$$

where P_L is the left-handed projection operator $(1-\gamma_5)/2$. From Eqs. (12) and (15), we see that the gauge (Yukawa) coupling constants are enhanced (suppressed) as v_Δ gets increased. These features are important to understand the decay property of the tripletlike Higgs bosons which is discussed in the next section.

We note that the interaction terms between quarks and tripletlike Higgs bosons except $H^{\pm\pm}$ are induced from the Yukawa interaction for the doublet Higgs field Φ via the small mixing denoted by α, β, and β' [22,28].

III. DECAY AND PRODUCTION OF $H^{\pm\pm}$

In this section, we discuss the decay and production of $H^{\pm\pm}$. For the decay of $H^{\pm\pm}$, we present the decay rates for all three decay modes. Especially, we discuss the diboson decay mode in detail, focusing on the cases where one or both of the W bosons are forced off shell. For the production of $H^{\pm\pm}$ at the LHC, we evaluate the cross sections in the LO and the NLO in QCD. We estimate the uncertainties of theoretical calculations by taking into account the scale ambiguity and the uncertainty from parton distribution functions (PDFs).

A. Decay branching ratio of $H^{\pm\pm}$

The decay properties of $H^{\pm\pm}$ strongly depend on v_Δ and the mass spectrum of the tripletlike Higgs bosons. For the case where $H^{\pm\pm}$ are the lightest among all the tripletlike Higgs bosons, i.e., $m_{A/H} \geq m_{H^\pm} \geq m_{H^{\pm\pm}}$, the same-sign dilepton decay $H^{\pm\pm} \to \ell^\pm\ell^\pm$ and the same-sign diboson decay $H^{\pm\pm} \to W^{\pm(*)}W^{\pm(*)}$ are possible. On the other hand, for the case where $H^{\pm\pm}$ are the heaviest, $m_{H^{\pm\pm}} > m_{H^\pm} > m_{A/H}$, another cascade-type decay $H^{\pm\pm} \to W^{\pm(*)}H^\pm$ is also possible.

For the diboson decay, in the case with $m_{H^{\pm\pm}} \geq 2m_W$, the tree-level decay rate is given by

$$\Gamma(H^{\pm\pm} \to W^\pm W^\pm) = \frac{\sqrt{2}G_F\sin^2\beta}{8\pi}m_{H^{\pm\pm}}^3 \times\left(1-4\frac{m_W^2}{m_{H^{\pm\pm}}^2}+12\frac{m_W^4}{m_{H^{\pm\pm}}^4}\right)\times\sqrt{1-\frac{4m_W^2}{m_{H^{\pm\pm}}^2}}. \tag{16}$$

Furthermore, the branching ratio for four-fermion final states is simply given by multiplying the decay branching ratio of the W bosons; i.e.,

$$\mathcal{B}(H^{\pm\pm}\to 4f) = \mathcal{B}(H^{\pm\pm}\to W^\pm W^\pm)\times\mathcal{B}(W\to f\bar{f}')\times\mathcal{B}(W\to f''\bar{f}''). \tag{17}$$

On the other hand, in the case with $m_{H^{\pm\pm}} < 2m_W$, at least one of the W bosons is forced off shell, and the decay rate given in Eq. (16) is no longer valid. Thus, the branching ratio of $H^{\pm\pm}$ into four-fermion final states is not simply described by Eq. (17). In order to clarify how the difference in the decay rate of $H^{\pm\pm}$ appears in the case with the off-shell W boson(s), we first consider the decay process of $H^{\pm\pm}$ into the four-lepton final states:

$$H^{\pm\pm} \to W^{\pm(*)}W^{\pm(*)} \to \ell^\pm\ell^\pm\nu\nu. \tag{18}$$

We can divide the decay modes into two cases: one is the same-flavor (s.f.) dilepton mode such as $e^\pm e^\pm$, $\mu^\pm\mu^\pm$, and the other is the different-flavor (d.f.) dilepton mode such as $e^\pm\mu^\pm$. In the s.f. dilepton decay, two Feynman diagrams drawn in Fig. 1 contribute, while only one Feynman diagram contributes in the d.f. dilepton decay. For each case, the partial decay width is calculated as

$$\Gamma(H^{\pm\pm}\to\ell^\pm\ell^\pm\nu\nu) = \Gamma_{\text{s.f.}} \equiv \frac{g^8v_\Delta^2}{m_{H^{\pm\pm}}}\frac{1}{4}\int d\Phi_4|\Delta_{13}\Delta_{24}+\Delta_{14}\Delta_{23}|^2(2p_1\cdot p_2)(2p_3\cdot p_4), \tag{19}$$

$$\Gamma(H^{\pm\pm}\to\ell^\pm\ell'^\pm\nu\nu') = \Gamma_{\text{d.f.}} \equiv \frac{g^8v_\Delta^2}{m_{H^{\pm\pm}}}\int d\Phi_4|\Delta_{13}\Delta_{24}|^2(2p_1\cdot p_2)(2p_3\cdot p_4), \tag{20}$$

where p_i^μ with $i=1,\ldots,4$ are the four momenta of the final-state leptons in the order of the last term in Eq. (18), $\Delta_{ij} = [(p_i+p_j)^2 - m_W^2 + im_W\Gamma_W]^{-1}$, and $\int d\Phi_4$ denotes full phase-space integration over the four-body final state.

We neglect the mass of leptons. The difference between the two widths exists only in the interference term in Eq. (19). Similarly, the partial decay width for the $\ell\nu jj$ channel is given by $\Gamma(H^{\pm\pm}\to\ell^\pm\nu jj) = 2N_c\Gamma_{\text{d.f.}}$ for each lepton

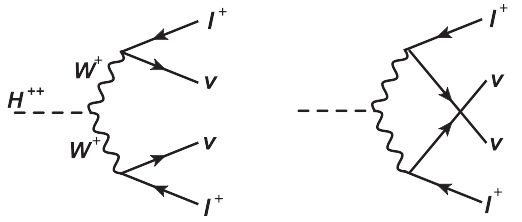

FIG. 1. Feynman diagrams of the $H^{++} \to \ell^+\ell^+\nu_\ell\nu_\ell$ decay. Both diagrams contribute for the same-flavor dilepton cases, while only one diagram contributes for the different-flavor dilepton cases.

flavor, where $N_c = 3$ is a number of color and a factor of 2 comes from (u, d) and (c, s).[3] In addition, there are two contributions for the partial decay width of the $jjjj$ channel, i.e., the same-flavor channel $\Gamma(H^{++} \to u\bar{d}u\bar{d}) = \Gamma(H^{++} \to c\bar{s}c\bar{s}) = \frac{N_c(N_c-1)}{2}\Gamma_{\rm d.f} + N_c\Gamma_{\rm s.f}$ and the different-flavor one $\Gamma(H^{++} \to u\bar{d}c\bar{s}) = N_c^2\Gamma_{\rm d.f.}$. Thus, the partial decay width into the four-jet mode is given as $\Gamma(H^{\pm\pm} \to jjjj) = 2N_c\Gamma_{\rm s.f} + N_c(2N_c-1)\Gamma_{\rm d.f.}$. In total, the sum of the decay width through $H^{\pm\pm} \to W^{\pm(*)}W^{\pm(*)}$ is given by $\Gamma_{H^{\pm\pm}} = (3+2N_c)\Gamma_{\rm s.f.} + (3+5N_c+2N_c^2)\Gamma_{\rm d.f.}$. We note that, in the case with $m_{H^{\pm\pm}} > 2m_W$ where both the W bosons can be on shell, $\Gamma_{\rm s.f.} = \Gamma_{\rm d.f.}/2$ is a good approximation by neglecting the interference term, and the branching ratios reduce to the product of branching ratios of the W bosons as in Eq. (17). Even for $m_{H^{\pm\pm}} > m_t + m_b$, the decay modes which include (t, b) can be safely neglected.

In Fig. 2, we plot the branching ratios for the decay of $H^{\pm\pm}$ into various four-fermion final states, such as $jjjj$, $\ell^\pm\nu jj$, and $\ell^\pm\ell^\pm\nu\nu$ with s.f. or d.f. leptons, as a function of $m_{H^{\pm\pm}}$. Notice that we neglect the dilepton decay and cascade decay channels here. It is found that the branching ratio of the s.f. $\ell^\pm\ell^\pm\nu\nu$ decay mode is enhanced by 80% for $m_{H^{\pm\pm}} \lesssim 90$ GeV, while by 10%–20% for 100 GeV $\lesssim m_{H^{\pm\pm}} \lesssim 160$ GeV. The ratio of all hadronic decay modes is also enhanced for $m_{H^{\pm\pm}} < 2m_W$ by 5%, while the ratio of $\ell^\pm\nu jj$ and d.f. $\ell^\pm\ell^\pm\nu\nu$ decay modes is suppressed by 10% and 5%, respectively. Therefore, for $m_{H^{\pm\pm}} < 2m_W$, the interference term can have a sizable and constructive contribution to the decay rate, and consequently the s.f. $\ell^\pm\ell^\pm\nu\nu$ decay becomes relatively

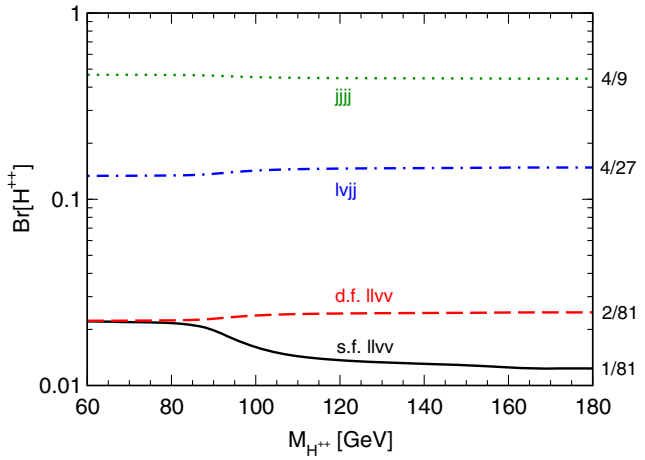

FIG. 2 (color online). Branching ratios of $H^{\pm\pm}$ into $jjjj$, $\ell^\pm\nu jj$, same-flavor and different-flavor $\ell^\pm\ell^\pm\nu\nu$ modes as a function of $m_{H^{\pm\pm}}$. In this plot, only the $H^{\pm\pm} \to W^{\pm(*)}W^{\pm(*)}$ mode is taken into account.

important. For the reference, on the right axis, we show the number of the branching ratio in the on-shell W boson limit for each decay mode, which apparently satisfies the probability conservation by $\mathcal{B}[jjjj] + 3\mathcal{B}[\ell\nu jj] + 3\mathcal{B}[\ell\nu\ell\nu] + 3\mathcal{B}[\ell\nu\ell'\nu'] = 1$, where the factor of 3 for the latter three terms comes from the number of lepton flavor.

The tree-level formula for the dilepton decay rate of $H^{\pm\pm}$ is given by

$$\Gamma(H^{\pm\pm} \to \ell_i^\pm\ell_j^\pm) = \frac{S_{ij}}{8\pi v_\Delta^2}|(m_\nu)_{ij}|^2 m_{H^{\pm\pm}}, \qquad (21)$$

where $S_{ij} = 1(1/2)$ for $i \neq j$ $(i = j)$.

For the cascade decay, taking into account the off shellness of the W boson, the tree-level formula is given by

$$\Gamma(H^{\pm\pm} \to H^\pm W^{\pm(*)}) = \frac{9g^4\cos^2\beta}{128\pi^3} m_{H^{\pm\pm}} G\left(\frac{m_{H^\pm}^2}{m_{H^{\pm\pm}}^2}, \frac{m_W^2}{m_{H^{\pm\pm}}^2}\right), \qquad (22)$$

where the phase-space functions are defined as

$$G(x,y) = \frac{1}{12y}\left\{2(x-1)^3 - 9(x^2-1)y + 6(x-1)y^2 - 3[1+(x-y)^2-2y]y\log x + 6(1+x-y)y\sqrt{-\lambda(x,y)}\left[\tan^{-1}\left(\frac{x-y-1}{\sqrt{-\lambda(x,y)}}\right) + \tan^{-1}\left(\frac{x+y-1}{\sqrt{-\lambda(x,y)}}\right)\right]\right\}, \qquad (23)$$

[3]We neglect the off-diagonal part of the Cabibbo-Kobayashi-Maskawa matrix.

$$\lambda(x,y) = 1 + x^2 + y^2 - 2xy - 2x - 2y. \qquad (24)$$

We note that the decay rate given in Eq. (22) is valid for the case with $m_{H^{\pm\pm}} - m_{H^\pm} < m_W$. In Ref. [37], it is shown that the mass difference larger than about 60 GeV is excluded by the electroweak precision data. Therefore, the on-shell decay mode of $H^{\pm\pm} \to H^\pm W^\pm$ is disfavored.

We then evaluate the decay of $H^{\pm\pm}$ for several values of v_Δ and $m_{H^{\pm\pm}}$ by taking into account all three decay channels: dilepton, diboson, and cascade decays. For the dilepton decay mode, we take all the elements of the neutrino mass matrix $(m_\nu)_{ij}$ 0.1 eV. In Fig. 3, we show the total decay width of $H^{\pm\pm}$ as a function of v_Δ for fixed values of $m_{H^{\pm\pm}} = 100$, 150, and 300 GeV (left panel) and as a function of $m_{H^{\pm\pm}}$ for fixed values of $v_\Delta = 1$ keV, 1 MeV, and 1 GeV (right panel). The mass of $H^\pm$ is taken to be the same as that of $H^{\pm\pm}$ so that the cascade decay mode is absent. As seen in the left panel, the total decay width takes its minimum at around $v_\Delta = 5$, 1, and 0.2 MeV in the case with $m_{H^{\pm\pm}} = 100$, 150, and 300 GeV, respectively. At these minima, the decay rates into the dilepton mode and the diboson mode are almost the same order. In the right panel, in the case where v_Δ is as small as 1 keV, the decay width increases linearly with $m_{H^{\pm\pm}}$, because the decay width is calculated dominantly from the dilepton decay rate given in Eq. (21). On the other hand, in the case where v_Δ is as large as 1 MeV or 1 GeV, the decay rate rapidly increases at around $m_{H^{\pm\pm}} = 160$ GeV, because of the threshold of the on-shell W boson pair. We note that the decay rate of 10^{-16} GeV corresponds to the decay length of about 1 m, so that $H^{\pm\pm}$ produced at colliders would decay inside a detector.

In Fig. 4, we show contour plots for the decay branching ratio of $H^{\pm\pm}$ in the v_Δ-Δm plane, where

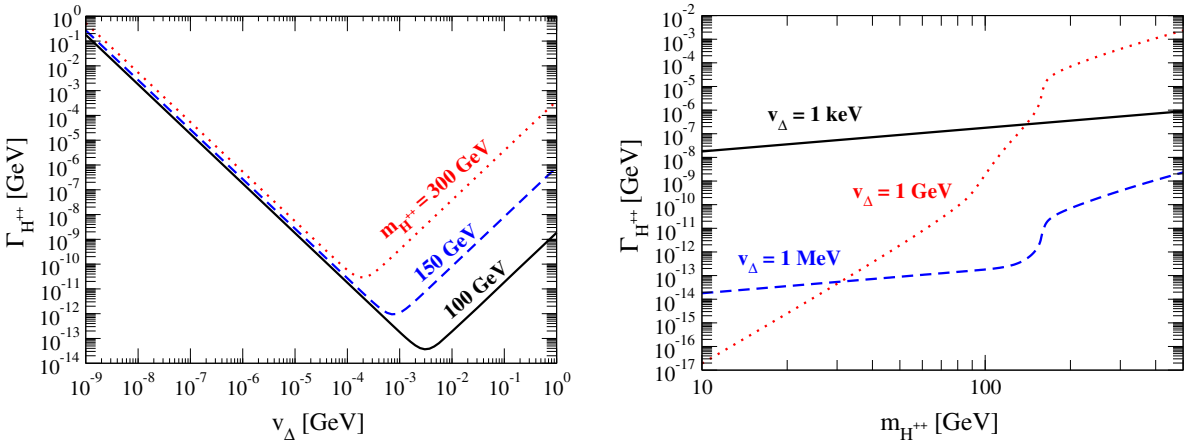

FIG. 3 (color online). The total width of $H^{\pm\pm}$. The left (right) panel shows the v_Δ ($m_{H^{\pm\pm}}$) dependence in the case with $m_{H^{\pm\pm}} = 100$, 150, and 300 GeV ($v_\Delta = 1$ keV, 1 MeV, and 1 GeV) in solid, dashed, and dotted lines, respectively. $m_{H^\pm} = m_{H^{\pm\pm}}$ is assumed, so that the cascade decay is absent.

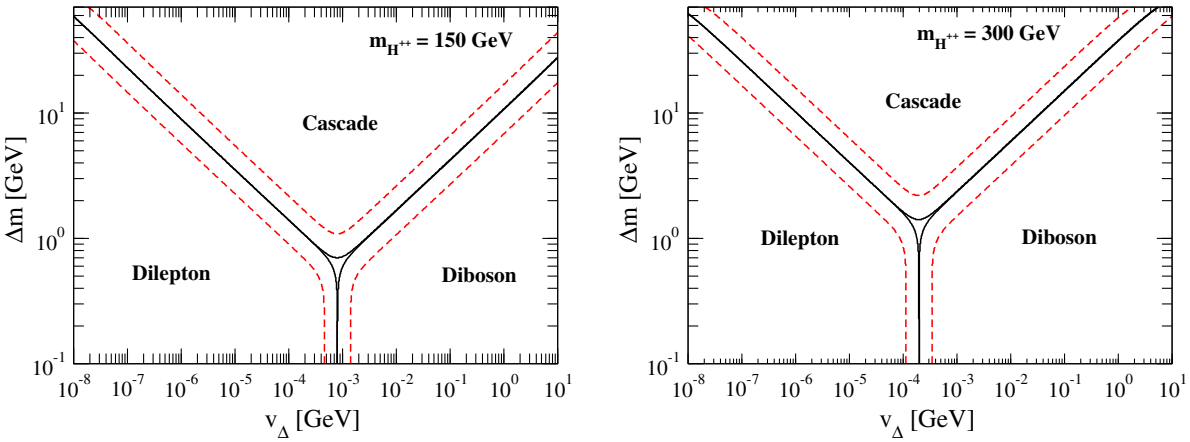

FIG. 4 (color online). Contour plot for the decay branching ratio of $H^{\pm\pm}$ on the v_Δ-$\Delta m(\equiv m_{H^{\pm\pm}} - m_{H^\pm})$ plane in the case of $m_{H^{\pm\pm}} = 150$ GeV (left panel) and $m_{H^{\pm\pm}} = 300$ GeV (right panel). The parameter regions on the black solid and red dashed lines give the 50% and 90% branching ratio for $H^{\pm\pm}$, respectively, where the decay mode is indicated inside the curves.

$\Delta m = m_{H^{\pm\pm}} - m_{H^{\pm}}$, in the case with $m_{H^{\pm\pm}} = 150$ (left panel) and 300 GeV (right panel) [27,28,31]. In each block bordered by the black (red) contours, the branching ratio for the decay mode indicated inside the block is greater than 50% (90%). We can observe that, by increasing v_Δ with fixing Δm smaller than about 1 GeV, the main decay mode is replaced from the dilepton mode to the diboson mode at $v_\Delta \simeq 0.1$–1 MeV. The regions where the diboson decay mode dominates are enlarged by increasing $m_{H^{\pm\pm}}$ from 150 to 300 GeV, due to the cubic power dependence of the diboson decay rate on $m_{H^{\pm\pm}}$ as expressed in Eq. (16). In the case where $H^{\pm\pm}$ are the lightest among the tripletlike Higgs bosons, the regions where the cascade decay dominates disappear.

We here comment on the decays of the other tripletlike Higgs bosons [22,28]. When v_Δ is smaller than about 1 MeV and $|\Delta m|$ is enough small, $H^\pm$, A, and H mainly decay into $\ell^\pm\nu$, $\nu\nu$, and $\nu\nu$, respectively, similarly to the decay of $H^{\pm\pm} \to \ell^\pm\ell^\pm$. When v_Δ is large, i.e., $v_\Delta \gtrsim 1$ MeV, $H^\pm$ mainly decay into $W^\pm Z$, $hW^\pm$, $\tau^\pm\nu$, and/or tb, while A mainly decays into hZ, $b\bar{b}$, $\tau^+\tau^-$, and/or $t\bar{t}$. The decay of H depends on the mixing angle α in addition to v_Δ and Δm. As seen in Eq. (6), $\tan 2\alpha$ is proportional to v_Δ/v_ϕ, so that small but nonzero α is typically provided at the same order as β and β', unless a large value of λ couplings is introduced. In such a case, the dominant decay mode of H can be WW, ZZ, hh, $b\bar{b}$, $\tau^+\tau^-$, and/or $t\bar{t}$. In the case with nonzero mass difference, a cascade decay $H \to H^\pm W^{\mp(*)}$ can take place.

In the following studies, we focus on the same-sign diboson decay scenario where $\mathcal{B}(H^{\pm\pm} \to W^{\pm(*)}W^{\pm(*)})$ is assumed to be almost 100%. This scenario can be realized in the case with rather large v_Δ with $m_{A/H} \geq m_{H^\pm} \geq m_{H^{\pm\pm}}$ or $\Delta m \ll 1$ GeV as discussed in this subsection.

B. Production cross sections at the LHC

The leading production processes of $H^{\pm\pm}$ at the LHC are

$$pp \to H^{++}H^{--} + X, \tag{25}$$

$$pp \to H^{\pm\pm}H^{\mp} + X. \tag{26}$$

In perturbative QCD, the total cross sections for these processes are expressed as

$$\sigma(pp \to H^{++}H^{--}) = \sum_q \int_{\tau_0}^1 d\tau \frac{d\mathcal{L}_{q\bar{q}}}{d\tau}(\tau,\mu_F)\hat{\sigma}_{q\bar{q}\to H^{++}H^{--}}(\tau s), \tag{27}$$

$$\sigma(pp \to H^{\pm\pm}H^{\mp}) = \sum_{q,q'} \int_{\tau_0}^1 d\tau \frac{d\mathcal{L}_{q\bar{q}'}}{d\tau}(\tau,\mu_F)\hat{\sigma}_{q\bar{q}'\to H^{\pm\pm}H^{\mp}}(\tau s), \tag{28}$$

where $\tau_0 = 4m^2_{H^{\pm\pm}}/s$ for Eq. (27) and $\tau_0 = (m_{H^{\pm\pm}} + m_{H^\pm})^2/s$ for Eq. (28). μ_F is the factorization scale. The partonic cross sections are given at the LO as

$$\hat{\sigma}_{q\bar{q}\to H^{++}H^{--}}(\hat{s}) = \frac{\pi\alpha^2}{9\hat{s}}(1-4x_{H^{\pm\pm}})^{\frac{3}{2}}\left[Q_H^2Q_q^2 + \frac{(1-x_Z)Q_HQ_qV_qV_H + \frac{1}{4}(V_q^2+A_q^2)V_H^2}{(1-x_Z)^2 + x_Z^2\Gamma_Z^2/m_Z^2}\right], \tag{29}$$

$$\hat{\sigma}_{q\bar{q}'\to H^{\pm\pm}H^{\mp}}(\hat{s}) = \frac{\pi\alpha^2\cos^2\beta}{36\hat{s}s_W^4}\left|\frac{1}{1-x_W(1+i\Gamma_W/m_W)}\right|^2\lambda^{3/2}(x_{H^{\pm\pm}},x_{H^\pm}), \tag{30}$$

where $x_i = m_i^2/\hat{s}$ ($i = W, Z, H^{\pm\pm}$, or $H^\pm$), $V_q = (T_q^3 - 2Q_qs_W^2)/(s_Wc_W)$, $A_q = T_q^3/(s_Wc_W)$, $Q_H = +2$ is the electric charge of H^{++}, $V_H = (1-2s_W^2)/(s_Wc_W)$, and $s_W = \sin\theta_W$, $c_W = \cos\theta_W$. The electric charge and the third component of the isospin for a fermion f are denoted by Q_f and T_f^3, respectively. The partonic luminosity functions are defined as

$$\frac{d\mathcal{L}_{q\bar{q}}}{d\tau}(\tau,\mu_F) = \int_0^1 dx_1\int_0^1 dx_2\delta(\tau-x_1x_2)\{f_q(x_1,\mu_F)f_{\bar{q}}(x_2,\mu_F) + f_{\bar{q}}(x_1,\mu_F)f_q(x_2,\mu_F)\}, \tag{31}$$

$$\frac{d\mathcal{L}_{q\bar{q}'}}{d\tau}(\tau,\mu_F) = \int_0^1 dx_1\int_0^1 dx_2\delta(\tau-x_1x_2)\{f_q(x_1,\mu_F)f_{\bar{q}'}(x_2,\mu_F) + f_{\bar{q}'}(x_1,\mu_F)f_q(x_2,\mu_F)\}. \tag{32}$$

The NLO QCD corrections to the total cross sections are calculated in Ref. [48]. We evaluate the LO and NLO total cross sections for the processes in Eqs. (25) and (26) at the LHC. In Fig. 5, we show the cross sections and K factors for $H^{++}H^{--}$ (left) and $H^{++}H^{-}$ (right) production at the LHC with $\sqrt{s} = 7$ TeV. We use CTEQ6L1 and CTEQ6M PDFs [49] for LO and NLO calculations, respectively, and vary the factorization scale μ_F and the renormalization scale μ_R, where the latter enters at the NLO, to see uncertainties of the cross section calculations. In the top panel, NLO (LO) cross sections are plotted in solid (dashed) lines as a function of $m_{H^{\pm\pm}}$.

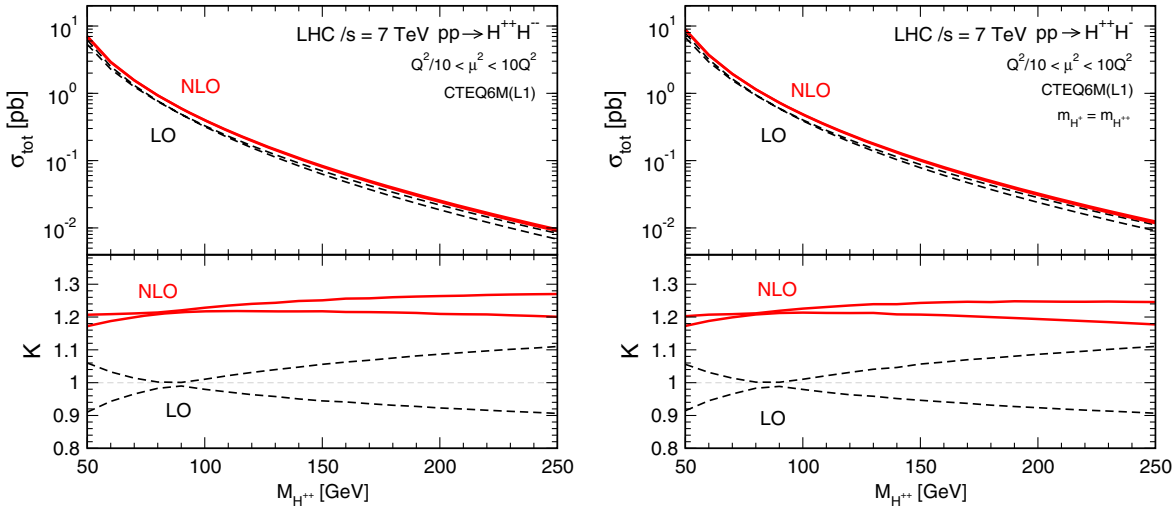

FIG. 5 (color online). Cross sections of $pp \to H^{++}H^{--}$ (left) and $pp \to H^{++}H^{-}$ (right) processes at the LHC with $\sqrt{s} = 7$ TeV evaluated at LO and NLO with CTEQ6L1 and CTEQ6M PDFs, respectively. The K factors are also plotted, which are defined as the cross sections evaluated at the LO and the NLO with varying the scales $\mu^2 = \mu_R^2 = \mu_F^2$ for $Q^2/10 < \mu^2 < 10Q^2$ divided by the LO cross section evaluated with $\mu^2 = Q^2$. For the second process, $m_{H^{\pm}} = m_{H^{\pm\pm}}$ is assumed.

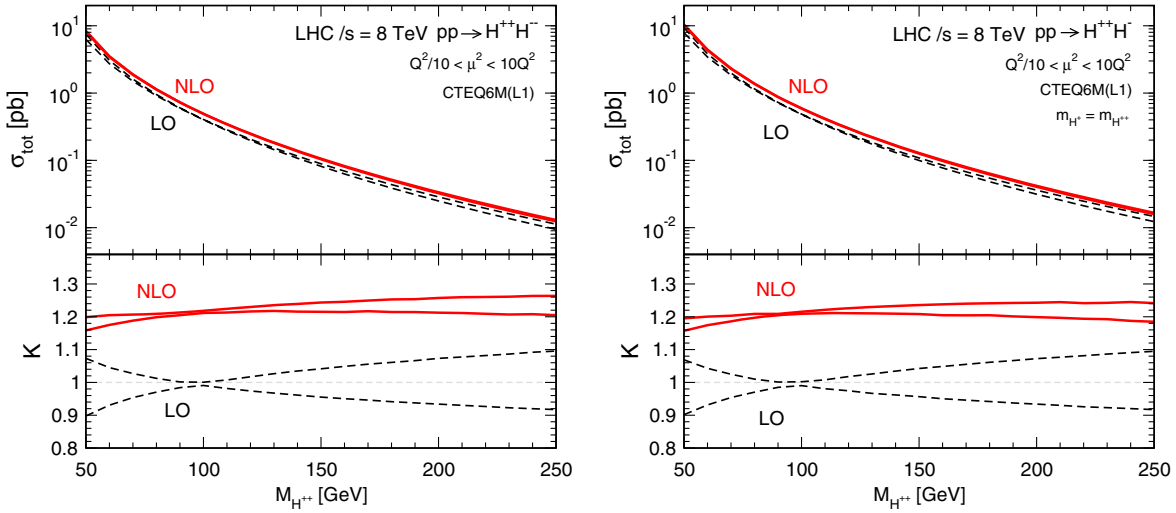

FIG. 6 (color online). The same figures as those in Fig. 5, but for $\sqrt{s} = 8$ TeV.

For each order, two lines are drawn which correspond to the maximum and minimal values by varying $\mu = \mu_R = \mu_F$ from $\mu^2 = Q^2/10$ to $\mu^2 = 10Q^2$, where Q is the invariant mass of the final-state scalar pair. Thus, the difference of the two lines indicates the uncertainty of the calculation by the choice of the scales. In the bottom panel, the corresponding K factors are plotted, which are defined as the ratios of those cross sections to the LO cross section evaluated with $\mu^2 = Q^2$. For both processes, the K factors are about 1.2. The scale uncertainties are typically the 5% (10%) level for the NLO (LO) calculation, while these are suppressed accidentally at around $m_{H^{\pm\pm}} \simeq 80$ GeV. The uncertainties from PDFs are found to be about 3% for the lower mass regions but about 10% for the higher mass regions.

We also show the same figures but for $\sqrt{s} = 8$ TeV in Fig. 6. For the reader's convenience, in the Appendix, we present tables for the cross sections and their uncertainties for all the processes in Eqs. (25) and (26) for various values of $m_{H^{\pm\pm}}$ and various collision energies at the LHC.

The other $H^{\pm\pm}$ production processes, i.e., the vector boson fusion $qQ \to q'Q'H^{\pm\pm}$ [18,24,30,35] and the weak boson associated production $q\bar{q}' \to W^{\pm *} \to H^{\pm\pm}W^{\mp}$, are induced by the $H^{\pm\pm}W^{\mp}W^{\mp}$ coupling which is proportional to v_Δ as shown in Eq. (12). Therefore, these production cross sections are suppressed due to $v_\Delta/v \ll 1$.

IV. BOUND ON THE MASS OF $H^{\pm\pm}$

In this section, we discuss the collider signals for the searches for $H^{\pm\pm}$ at LEP and the LHC in the diboson decay

scenario. Since there have been no dedicated studies in past experiments, to our knowledge, we start to consider the experimental constraint from relatively small mass regions by using the precise measurement on the Z boson width at the LEP I experiment. Expected signal events for $H^{\pm\pm}$ in the $e^+e^- \to H^{++}H^{--}$ process are studied for the LEP II energy and luminosity. After that, we study the constraint on $H^{\pm\pm}$ in the inclusive same-sign dilepton events at the LHC.

A. LEP I

The LEP experiment was operated with the electron-positron collision at the center-of-mass energy on the Z boson mass (LEP I) and up to about 209 GeV (LEP II). At the LEP I experiment, the total decay width of the Z boson has been precisely measured [50]. The measurement can be used to constrain $H^{\pm\pm}$ whose mass is smaller than half of m_Z independently of the decay modes of $H^{\pm\pm}$. For $m_{H^{\pm\pm}}$ smaller than half of m_Z, the total decay width of the Z boson receives a sizable correction from the partial width for the $Z \to H^{++}H^{--}$ decay as

$$\Gamma_{Z\to H^{++}H^{--}} = \frac{G_F m_Z^3}{6\pi\sqrt{2}}(1-2s_W^2)^2\left(1-\frac{4m_{H^{\pm\pm}}^2}{m_Z^2}\right)^{\frac{3}{2}}.$$

Using the current experimental data and the SM prediction for the Z boson width [47], $\Gamma_Z(\mathrm{exp}) = 2.4952 \pm 0.0023$ GeV and $\Gamma_Z(\mathrm{SM}) = 2.4960 \pm 0.0002$ GeV, respectively, we obtain the lower bound $m_{H^{\pm\pm}} > 42.9$ GeV at the 95% C.L.

B. LEP II

For $m_Z/2 < m_{H^{\pm\pm}} < \sqrt{s}/2$, a pair production process of $H^{\pm\pm}$, $e^+e^- \to H^{++}H^{--}$, is utilized to search for $H^{\pm\pm}$ at the LEP II experiment. The total cross section for this process is given by

$$\sigma_{ee}(s) = \frac{\pi\alpha^2}{3s}(1-4x_{H^{\pm\pm}})^{\frac{3}{2}}\left[Q_H^2Q_e^2 + \frac{(1-x_Z)Q_HQ_eV_eV_H + \frac{1}{4}(V_e^2+A_e^2)V_H^2}{(1-x_Z)^2 + x_Z^2\Gamma_Z^2/m_Z^2}\right], \tag{33}$$

where $V_e = (T_e^3 - 2Q_e s_W^2)/(s_W c_W)$ and $A_e = T_e^3/(s_W c_W)$. The searches for $H^{\pm\pm}$ in the dilepton decay mode have been performed at the LEP experiment [39]. We consider the searches for $H^{\pm\pm}$ in the diboson decay scenario. Through the decays of $H^{\pm\pm}$ into the (off-shell) W bosons, it subsequently leads to various exotic signals, such as 8-jets, lepton plus 6-jets plus missing energy, same-sign or opposite-sign dilepton plus 4-jets plus missing energy, trilepton plus 2-jets plus missing energy, and tetralepton plus missing energy. Produced numbers of events for these signals are estimated to be

$$N(\text{8-jets}) = \sigma_{ee}\cdot\mathcal{B}(H^{\pm\pm}\to jjjj)^2\cdot\int\mathcal{L}dt, \tag{34}$$

$$N(\ell^\pm E_T + \text{6-jets}) = \sigma_{ee}\cdot 2\mathcal{B}(H^{\pm\pm}\to jjjj)\mathcal{B}(H^{\pm\pm}\to \ell\nu jj)\cdot\int\mathcal{L}dt, \tag{35}$$

$$N(\ell^\pm\ell^\pm E_T + \text{4-jets}) = \sigma_{ee}\cdot 2\mathcal{B}(H^{\pm\pm}\to \ell\ell\nu\nu)\mathcal{B}(H^{\pm\pm}\to jjjj)\cdot\int\mathcal{L}dt, \tag{36}$$

$$N(\ell^\pm\ell^\mp E_T + \text{4-jets}) = \sigma_{ee}\cdot \mathcal{B}(H^{\pm\pm}\to \ell\nu jj)^2\cdot\int\mathcal{L}dt, \tag{37}$$

$$N(\ell^\pm\ell^\pm\ell^\mp E_T + \text{2-jets}) = \sigma_{ee}\cdot 2\mathcal{B}(H^{\pm\pm}\to \ell\ell\nu\nu)\mathcal{B}(H^{\pm\pm}\to \ell\nu jj)\cdot\int\mathcal{L}dt, \tag{38}$$

$$N(\ell^+\ell^+\ell^-\ell^- E_T) = \sigma_{ee}\cdot \mathcal{B}(H^{\pm\pm}\to \ell\ell\nu\nu)^2\cdot\int\mathcal{L}dt, \tag{39}$$

where $\ell = e, \mu$ but the signals with τ's are neglected for simplicity.

In Fig. 7, we plot the expected number of events for these signals as a function of $m_{H^{\pm\pm}}$ at the LEP II experiment. We calculate the expected number of events by collecting the cross sections for various collision energies and integrated luminosities listed in Table I [51]. As a reference, the number of event for the total $H^{++}H^{--}$ production is also plotted.

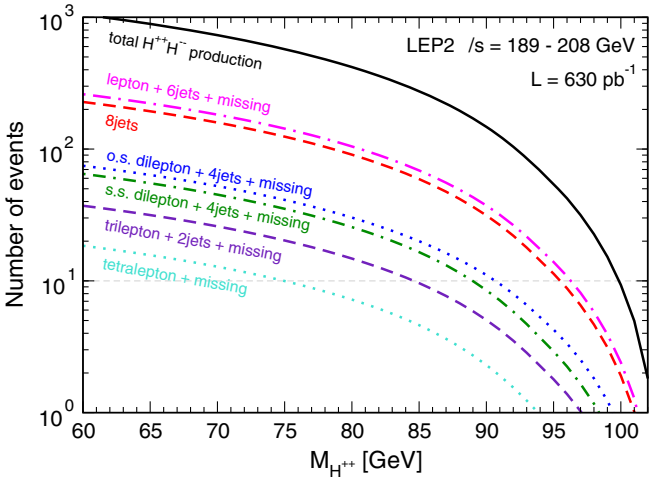

FIG. 7 (color online). Estimated number of events for various signals in the $e^+e^- \to H^{++}H^{--}$ process in the diboson decay scenario at the LEP II experiments as a function of $m_{H^{\pm\pm}}$. The total number of events for the $e^+e^- \to H^{++}H^{--}$ production is also plotted. The collision energies and the integrated luminosities collected at the LEP II experiments are listed in Table I.

Although the signal of a tetralepton plus missing energy can be compared with the results for the $e^+e^- \to H^{++}H^{--} \to \ell^+\ell^+\ell^-\ell^-$ search [39] which requires the four charged leptons exclusively, no substantial bound can been derived in the diboson decay scenario because of the suppression of the number of signal events by $\mathcal{B}(H^{\pm\pm} \to \ell^\pm\ell^\pm\nu\nu)^2$ whose numerical value is figured in Fig. 2. Up to our knowledge, there have been no dedicated studies on these signals as direct searches for the same-sign diboson decay of $H^{\pm\pm}$ at the LEP II experiment.

For the signals which include same-sign dileptons in Eq. (36) or trileptons in Eq. (36), we wonder if there can be a chance to find evidence for $H^{\pm\pm}$ at the LEP II experiment. For example, if we assume that these signals can be discovered if the expected number of events exceeds ten, $m_{H^{\pm\pm}} \simeq 85$–90 GeV can be explored at the LEP II experiment. The signal of a lepton plus 6-jets plus missing energy is similar to the process $e^+e^- \to W^+W^- \to \ell^\pm\nu jj$ [52]. Because the invariant mass of jets is close to m_W for the latter process, the separation of the two processes seems possible. The detection of the 8-jets event should be suffered by a background contribution from QCD events and W^+W^- production in the all hadronic decays channel [51]. However, detailed analysis on the event topology variables or shape variables, such as thrust or acoplanarity, may be used to discriminate the signal events from the background [53,54]. To draw a concrete conclusion, one needs more detailed studies on the detection efficiencies for these signals, a realistic estimation of the background processes, etc., which are beyond the scope of this paper. Analyses using the real data at the LEP II experiments are also desired.

TABLE I. Collision energies $\sqrt{s}$ and integrated luminosities $\mathcal{L}$ at the LEP II experiments [51].

$\sqrt{s}$ [GeV]	188.6	191.6	195.5	199.6	201.8	204.8	206.5	208.0
$\mathcal{L}$ [pb^{-1}]	176.8	29.8	84.1	83.3	37.1	79.0	130.5	8.6

Consequently, by using the data as far as we could handle, we obtain the bound $m_{H^{\pm\pm}} > 43$ GeV from the Γ_Z measurement at the LEP experiment, although the bound is quite solid, i.e., independent of the decay of $H^{\pm\pm}$.

C. Bound from LHC data

Let us consider the constraint on $m_{H^{\pm\pm}}$ in the diboson decay scenario by using the current LHC data. As explained in Sec. II B, the main production mode for $H^{\pm\pm}$ is the pair production $pp \to Z/\gamma^* \to H^{++}H^{--}$ and the associated production $pp \to W^\pm \to H^{\pm\pm}H^\mp$ at the LHC. Among the various final states in the diboson decay of $H^{\pm\pm}$, the $\ell^\pm\ell^\pm\nu\nu$ final state brings the most clean signature at colliders, since the background contribution can be suppressed for the signals with same-sign dileptons. Thus, we consider that the experimental signatures suited for the discovery are

$$\begin{aligned} pp &\to H^{++}H^{--} + X \to \ell^\pm\ell^\pm E_T + X, \\ pp &\to H^{\pm\pm}H^\mp + X \to \ell^\pm\ell^\pm E_T + X, \end{aligned} \tag{40}$$

where $\ell^\pm$ denotes $e^\pm$ or $\mu^\pm$. The theoretical cross section for the same-sign dilepton signal can be estimated to be

$$\begin{aligned} \sigma(\ell^\pm\ell^\pm E_T + X) = [\sigma(H^{++}H^{--} + X) + \sigma(H^{\pm\pm}H^\mp + X)] \\ \times \mathcal{B}(H^{\pm\pm} \to \ell^\pm\ell^\pm\nu\nu). \end{aligned} \tag{41}$$

To obtain the direct bound on $H^{\pm\pm}$, we apply the results of the same-sign dilepton search reported by the ATLAS Collaboration [45] using the data at the collision energy of 7 TeV and the integrated luminosity of 4.7 fb^{-1}. From the data, 95% C.L. upper limits N_{95} for the event number for the process including the same-sign dilepton have been derived. In Ref. [45], the limits are separately given for $e^\pm e^\pm$, $\mu^\pm\mu^\pm$, and $e^\pm\mu^\pm$ channels after imposing several choices of the cut on the invariant mass $M_{\ell\ell}$ of the same-sign dilepton. The 95% C.L. limit for the fiducial cross section $\sigma^{95}_{\rm fid}$ is obtained by

$$\sigma^{95}_{\rm fid} = \frac{N_{95}}{\int \mathcal{L}dt \cdot \varepsilon_{\rm fid}}, \tag{42}$$

where $\varepsilon_{\rm fid}$ is the efficiency for detecting events within the detector acceptance and $\int \mathcal{L}dt$ is the integrated luminosity 4.7 fb^{-1}. The efficiencies are also given in Ref. [45] reading 43%–65% for the ee channel, 55%–70% for the $e\mu$ channel, and 59%–72% for the $\mu\mu$ channel depending on the assumption about momentum distributions of the

TABLE II. Table of the total cross sections, branching ratio of $H^{\pm\pm}$, and the efficiencies of acceptance and kinematical cuts for the $\mu^+\mu^+$ searches at the LHC with 7 TeV for $m_{H^{\pm\pm}} = 40$–100 GeV. The resulting fiducial cross section is also listed.

$m_{H^{\pm\pm}}$	40	50	60	70	80	90	100	[GeV]
$\sigma_{\rm tot}^{\rm NLO}(pp \to H^{++}H^{--})$	120.	6.95	2.90	1.56	0.93	0.594	0.398	[pb]
$\sigma_{\rm tot}^{\rm NLO}(pp \to H^{++}H^{-})$ $[m_{H^{\pm}} = m_{H^{\pm\pm}}]$	65.	8.76	3.69	1.94	1.14	0.725	0.485	[pb]
$\mathcal{B}(H^{++} \to \mu^+\mu^+\nu\nu)$	2.22	2.22	2.21	2.19	2.16	1.98	1.61	[%]
$\epsilon_{\rm A}$ ($p_T^{\mu} > 20$ GeV and $\lvert\eta_{\mu}\rvert < 2.5$)	0.63	6.1	12.	17.	22.	24.	23.	[%]
$\epsilon_{\rm A}$ ($M_{\mu\mu} > 15$ GeV)	78.	89.	94.	96.	98.	98.	99.	[%]
$\sigma_{\rm fid}(pp \to \mu^+\mu^+ + X)$ $[m_{H^{\pm}} = m_{H^{\pm\pm}}]$	20.2	18.9	16.4	12.5	9.6	6.1	3.2	[fb]

charged leptons. We find that the data for the $\mu^+\mu^+$ channel with the invariant-mass cut $M_{\ell\ell} > 15$ GeV give the most severe constraint on $m_{H^{\pm\pm}}$. Thus, hereafter, we present a detailed comparison of $\sigma_{\rm fid}^{95}$ given in Ref. [45] with the fiducial cross section evaluated by ourselves for the $\mu^+\mu^+$ channel with a cut of $M_{\ell\ell} > 15$ GeV. Theoretical estimation of the fiducial cross section is given by

$$\sigma_{\rm fid} = \sigma_{\rm tot} \cdot \mathcal{B} \cdot \epsilon_{\rm A}, \tag{43}$$

where $\epsilon_{\rm A}$ is the combined efficiency of kinematical acceptance and kinematical cuts. In Table II, our estimation for each factor is summarized. In the first and second rows, the total cross sections for $pp \to H^{++}H^{--}$ and $pp \to H^{++}H^{-}$ processes at the NLO are listed as a function of $m_{H^{\pm\pm}}$, where $m_{H^{\pm}} = m_{H^{\pm\pm}}$ is assumed for the second process. We set 5% uncertainty for the cross sections independently of $m_{H^{\pm\pm}}$ from the scale uncertainty and the PDF uncertainty. The branching ratio of $H^{\pm\pm}$ into the same-sign dimuon plus missing momentum is also listed in the third row in Table II.

The efficiencies of detector acceptance and kinematical cuts are separately estimated by using the Monte Carlo simulation at the parton level. In order to generate the signal events, we use MADGRAPH5 [55] and CTEQ6L PDFs [49]. In Fig. 8, we show the distributions for the signal events in the transverse momentum of a muon, the missing transverse momentum, and $M_{\mu\mu}$ for $m_{H^{\pm\pm}} = 40$–100 GeV to check the shape of the distributions and their mass dependence. According to Ref. [45], the kinematical cuts by detector acceptance are taken as

$$p_T^{\mu} > 20 \text{ GeV}, \qquad |\eta_{\mu}| < 2.5, \tag{44}$$

where p_T^{μ} and η_{μ} represent the transverse momentum and the pseudorapidity of a muon, respectively. In addition, a cut on $M_{\mu\mu} > 15$ GeV is applied. In the fourth and fifth rows in Table II, the efficiencies by the kinematical acceptance for muons and that by the kinematical cut on the dimuon invariant mass are listed, respectively. Because only the muon momenta are measured, our parton-level analysis is expected to be a good approximation to the realistic detector-level observation. Finally, in the last row, we list the fiducial cross section as a function of $m_{H^{\pm\pm}}$, calculated by using the numbers in the upper rows. The fiducial cross section takes its maximum value at around $m_{H^{\pm\pm}} = 40$ GeV, because that for a lower mass is significantly reduced by the acceptance cut.

In Fig. 9, the fiducial cross section for the $\mu^+\mu^+$ events is plotted as a function of $m_{H^{\pm\pm}}$ by a dark green band, where its width indicates 5% uncertainty for the total cross section at the NLO. For the comparison, the LO results previously

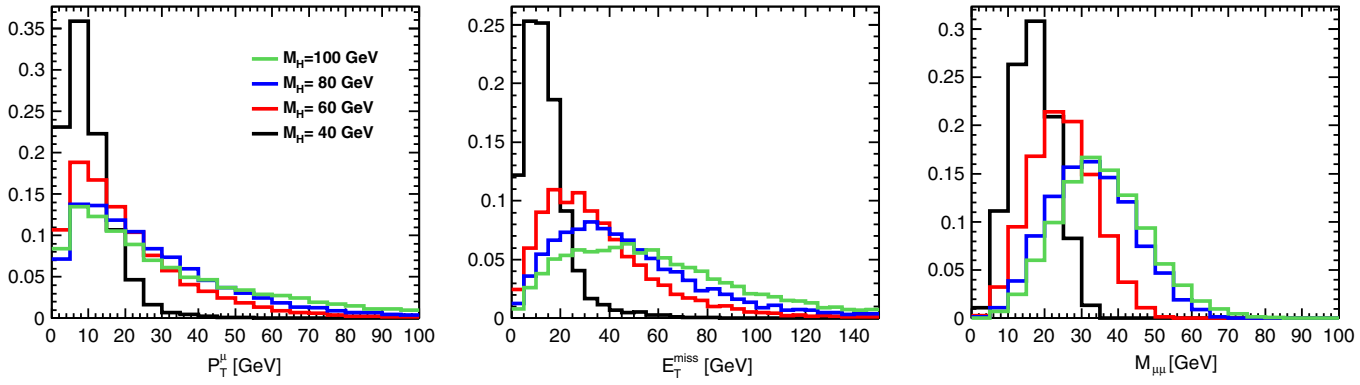

FIG. 8 (color online). Normalized distributions of p_T of muons, missing transverse momentum, and the invariant mass of the same-sign dimuon for the inclusive $pp \to (H^{++} \to \mu^+\mu^+\nu\nu)X$ process at the LHC with $\sqrt{s} = 7$ TeV. Distributions are evaluated by using MADGRAPH [55] with $m_{H^{\pm\pm}} = 40$, 60, 80, and 100 GeV.

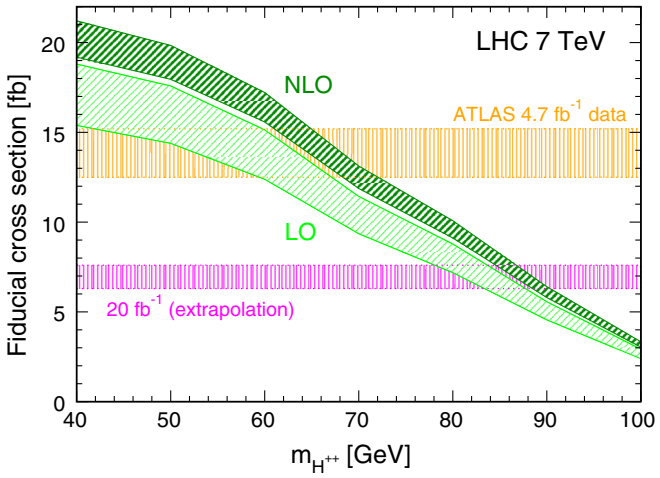

FIG. 9 (color online). The fiducial cross section for the $\mu^+\mu^+$ events at the LHC with $\sqrt{s} = 7$ TeV as a function of $m_{H^{\pm\pm}}$. Dark green and light green bands show the estimated fiducial cross sections at the NLO and LO, respectively. The widths of the band come from the 5% (10%) uncertainty for the production cross sections at the NLO (LO). The horizontal thick (thin) band shows the (expected) 95% C.L. upper limit from the data with the integrated luminosity of 4.7 fb^{-1} (20 fb^{-1}).

obtained in Ref. [33] are also shown in the light green band where 10% theory uncertainty is taken into account. An orange-shaded band gives the 95% C.L. upper limit for the fiducial cross section obtained in Ref. [45] by using 4.7 fb^{-1} data. The width of the data band comes from the uncertainty of $\varepsilon_{\rm fid}$ for the $\mu\mu$ system between 59% and 72% [45]. By taking a conservative examination, $H^{\pm\pm}$ is excluded for $m_{H^{\pm\pm}} \lesssim 60$–68 GeV in the diboson decay scenario, depending on the value of $\epsilon_{\rm fid}$ in Ref. [45]. We emphasize again that this is the first verification by using the collider data on the searches for $H^{\pm\pm}$ in the diboson scenario. We find that a stronger mass bound is obtained by using the LHC data more than the bound obtained via the Γ_Z measurement at the LEP experiment. The red-shaded band is drawn by extrapolating the ATLAS results to those for 20 fb^{-1} by assuming that the upper limit of the cross section $\sigma^{95}_{\rm fid}$ becomes small by a factor of 2. By comparing the extrapolated band with the theoretical cross section, we obtain that the regions of $m_{H^{\pm\pm}} \lesssim 85$–90 GeV can be surveyed by using the existing LHC data with 20 fb^{-1}. We note that the difference of the signal cross sections from 7 to 8 TeV is not taken into account for this extrapolation, since we do not know how the background cross sections scale at the same time. The analysis for the 8 TeV run should be revised by taking into account the change of these cross sections as well as the efficiencies provided from the experimental measurements.

We remark that the lower bound obtained in this analysis can be improved by taking into account the following: (i) The other source of extra $H^{\pm\pm}$ from the decay of $H^\pm$ is not considered here, for simplicity, since the decay rate of $H^\pm \to H^{\pm\pm}W^\mp$ depends on the other parameters in the model [28]. To count the $H^{\pm\pm}$ production from the decay of $H^\pm$, all the processes of $H^\pm$ production have to be also taken into account [26,28,29,31], such as $pp \to H^+H^-$, $pp \to H^\pm H$, and $pp \to H^\pm A$. (ii) Although we have studied the same-sign dileptons only from the decay of $H^{\pm\pm}$, they can also appear in the decay of $H^\pm$; e.g., $H^\pm \to W^\pm Z \to \ell^\pm\ell^+\ell^-\nu$ [28]. However, the decay of $H^\pm$ also strongly depends on the mass difference among the triplet Higgs bosons, $\Delta m = m_{H^\pm} - m_{H^{\pm\pm}}$, so that we here neglect these contributions as a conservative assumption. (iii) The mass bound obtained in our analysis is somewhat lower than that estimated in Ref. [30] for the same collision energy and integrated luminosity. This is partially because of the difference between their estimation for the background events and the real data and partially because of the difference of the analysis cuts. Although we have used the experimental data for the inclusive same-sign dilepton production, it has been studied that a requirement of relatively hard jets in addition to the same-sign dilepton can enhance the significance for discovering $H^{\pm\pm}$ [30,36]. In the future LHC run with $\sqrt{s} = 13$–14 TeV, the mass bound can be further improved by such an optimized analysis.

Finally, we comment on further observations after the discovery of $H^{\pm\pm}$, such as the determination of its properties and searches for the other tripletlike Higgs bosons. If $H^{\pm\pm}$ are discovered by the $\ell^\pm\ell^\pm\nu\nu$ events, the observations of the other signals which come from the hadronic decays of the (off-shell) W bosons are important to indeed conclude the diboson decay of $H^{\pm\pm}$. The electric charge of $H^{\pm\pm}$ shall be determined from the charges of the same-sign dilepton as discovery signals in either the dilepton decay scenario or the diboson decay scenario. In the dilepton decay scenario, the mass of $H^{\pm\pm}$ can be easily determined by the sharp peak in the invariant-mass distribution of the same-sign dilepton. Angular distributions of leptons discriminate the spin of $H^{\pm\pm}$. In addition, if $H^{\pm\pm} \to \tau^\pm\tau^\pm$ decays are available, the spin of $H^{\pm\pm}$ can be directly observed by using the spin correlation of the two reconstructed τ leptons [56]. On the other hand, in the diboson decay scenario, the determination of the mass of $H^{\pm\pm}$ is not straightforward but still possible at hadron colliders by using the end-point behavior of the transverse mass distribution constructed from the dilepton momenta and the missing transverse momentum [28]. Moreover, the method using the lepton energy distribution [57] may be also applicable, since clean signal events can be extracted in the sense of the kinematical cuts for leptons and the SM background contributions. Observation of the spin of $H^{\pm\pm}$ may be performed in the same method as the observation of the spin-0 nature of the SM-like Higgs bosons at the LHC [3]. The searches for the other tripletlike Higgs bosons will be performed at the future LHC run and also at future lepton colliders, such as the International Linear Collider

TABLE III. Total cross sections at the NLO with CT10 PDFs for $H^{\pm\pm}$ production processes at the LHC with $\sqrt{s} = 7$ TeV. The errors show the uncertainty by varying the scale $\mu = \mu_R = \mu_F$ as $Q^2/10 < \mu^2 < 10Q^2$ and the uncertainty in the PDFs, in order. For the second and third processes, $m_{H^\pm} = m_{H^{\pm\pm}}$ is assumed.

LHC $\sqrt{s} = 7$ TeV, NLO with CT10 PDFs						
Mass [GeV]	$\sigma(H^{++}H^{--})$ [pb]		$\sigma(H^{++}H^{-})$ [pb]		$\sigma(H^{+}H^{--})$ [pb]	
50	7.19×10^{0}	$^{+1.7\%\ +3.2\%}_{-0.8\%\ -3.5\%}$	9.01×10^{0}	$^{+1.6\%\ +3.8\%}_{-0.7\%\ -4.4\%}$	5.60×10^{0}	$^{+1.8\%\ +3.7\%}_{-0.7\%\ -4.2\%}$
60	2.98×10^{0}	$^{+1.1\%\ +3.4\%}_{-0.3\%\ -3.6\%}$	3.78×10^{0}	$^{+1.0\%\ +3.9\%}_{-0.3\%\ -4.5\%}$	2.26×10^{0}	$^{+1.2\%\ +3.9\%}_{-0.4\%\ -4.3\%}$
70	1.60×10^{0}	$^{+0.6\%\ +3.4\%}_{-0.1\%\ -3.8\%}$	1.98×10^{0}	$^{+0.5\%\ +4.0\%}_{-0.1\%\ -4.7\%}$	1.14×10^{0}	$^{+0.7\%\ +4.0\%}_{-0.1\%\ -4.4\%}$
80	9.51×10^{-1}	$^{+0.4\%\ +3.4\%}_{-0.0\%\ -4.0\%}$	1.16×10^{0}	$^{+0.4\%\ +4.1\%}_{-0.0\%\ -4.9\%}$	6.50×10^{-1}	$^{+0.3\%\ +4.2\%}_{-0.0\%\ -4.7\%}$
90	6.07×10^{-1}	$^{+0.5\%\ +3.5\%}_{-0.1\%\ -4.2\%}$	7.37×10^{-1}	$^{+0.5\%\ +4.1\%}_{-0.2\%\ -5.1\%}$	4.00×10^{-1}	$^{+0.5\%\ +4.4\%}_{-0.1\%\ -4.9\%}$
100	4.06×10^{-1}	$^{+0.7\%\ +3.7\%}_{-0.4\%\ -4.3\%}$	4.92×10^{-1}	$^{+0.7\%\ +4.2\%}_{-0.5\%\ -5.3\%}$	2.60×10^{-1}	$^{+0.8\%\ +4.5\%}_{-0.4\%\ -5.2\%}$
120	2.01×10^{-1}	$^{+1.0\%\ +3.9\%}_{-1.0\%\ -4.7\%}$	2.44×10^{-1}	$^{+1.1\%\ +4.4\%}_{-1.1\%\ -5.8\%}$	1.23×10^{-1}	$^{+1.1\%\ +5.0\%}_{-1.0\%\ -5.7\%}$
140	1.10×10^{-1}	$^{+1.3\%\ +4.1\%}_{-1.5\%\ -5.0\%}$	1.34×10^{-1}	$^{+1.3\%\ +4.6\%}_{-1.5\%\ -6.3\%}$	6.45×10^{-2}	$^{+1.4\%\ +5.3\%}_{-1.5\%\ -6.2\%}$
160	6.41×10^{-2}	$^{+1.5\%\ +4.3\%}_{-1.9\%\ -5.4\%}$	7.91×10^{-2}	$^{+1.6\%\ +5.0\%}_{-1.9\%\ -6.7\%}$	3.66×10^{-2}	$^{+1.6\%\ +5.7\%}_{-2.0\%\ -6.6\%}$
180	3.94×10^{-2}	$^{+1.8\%\ +4.6\%}_{-2.3\%\ -5.8\%}$	4.91×10^{-2}	$^{+1.8\%\ +5.2\%}_{-2.3\%\ -7.2\%}$	2.19×10^{-2}	$^{+1.9\%\ +6.1\%}_{-2.3\%\ -7.1\%}$
200	2.52×10^{-2}	$^{+2.0\%\ +4.8\%}_{-2.6\%\ -6.1\%}$	3.18×10^{-2}	$^{+2.0\%\ +5.5\%}_{-2.7\%\ -7.7\%}$	1.37×10^{-2}	$^{+2.1\%\ +6.5\%}_{-2.7\%\ -7.5\%}$
250	9.35×10^{-3}	$^{+2.5\%\ +5.6\%}_{-3.4\%\ -6.9\%}$	1.21×10^{-2}	$^{+2.5\%\ +6.5\%}_{-3.5\%\ -8.9\%}$	4.84×10^{-3}	$^{+2.6\%\ +7.7\%}_{-3.5\%\ -8.5\%}$
300	3.95×10^{-3}	$^{+3.0\%\ +6.3\%}_{-4.1\%\ -7.7\%}$	5.23×10^{-3}	$^{+3.0\%\ +7.6\%}_{-4.1\%\ -10.3\%}$	1.96×10^{-3}	$^{+3.1\%\ +8.8\%}_{-4.2\%\ -9.6\%}$
350	1.82×10^{-3}	$^{+3.5\%\ +7.1\%}_{-4.7\%\ -8.6\%}$	2.45×10^{-3}	$^{+3.5\%\ +9.1\%}_{-4.8\%\ -11.5\%}$	8.74×10^{-4}	$^{+3.6\%\ +10.2\%}_{-4.8\%\ -10.7\%}$
400	8.91×10^{-4}	$^{+3.9\%\ +8.1\%}_{-5.2\%\ -9.4\%}$	1.22×10^{-3}	$^{+4.0\%\ +10.7\%}_{-5.4\%\ -13.0\%}$	4.16×10^{-4}	$^{+4.0\%\ +11.9\%}_{-5.3\%\ -12.0\%}$

(ILC) [58] and Compact Linear Collider (CLIC) [59,60]. Since the heavier tripletlike bosons would decay in the cascade type, the searches at the LHC may be difficult and there can be an advantage for the searches at future lepton colliders [61]. Searches for the tripletlike Higgs bosons at photon colliders are also discussed in Refs. [16,62].

We close this section with comments on the diboson decay of $H^{\pm\pm}$ in the other $\mathrm{SU}(2)_L$ multiplet. In general, an $\mathrm{SU}(2)_L$ scalar multiplet φ which contains both the doubly charged $\varphi^{\pm\pm}$ and neutral φ^0 components can have the $\varphi^{\pm\pm}W^{\mp}W^{\mp}$ vertex at tree level, when φ^0 acquires a nonzero VEV.[4] Although the bound obtained in this paper is limited for the triplet scalar, the same searches can be applied to them by adopting the appropriate production cross section and branching ratio.

V. CONCLUSION

We have investigated the collider phenomenology of $H^{\pm\pm}$ in the HTM, focusing on the scenario where $H^{\pm\pm}$ mainly decay into the same-sign diboson. Such a diboson decay scenario can be realized in the case with $v_\Delta > 0.1$–1 MeV and $\Delta m \lesssim 1$ GeV as shown in Fig. 4. We have shown that the decay branching ratio for the $H^{\pm\pm} \to \ell^{\pm}\ell^{\pm}\nu\nu$ decay with a s.f. dilepton is enhanced by up to 80% for $m_{H^{\pm\pm}} < 2m_W$ due to the interference effect. Total production cross sections of $pp \to H^{++}H^{--}$ and $pp \to H^{\pm\pm}H^{\mp}$ are calculated up to the NLO in QCD. The predicted cross sections are enhanced by about 20% from those at the LO. These arguments are found to be important to search for $H^{\pm\pm}$ in the diboson decay scenario in relatively small mass regions.

Since there have been no dedicated studies for the search for $H^{\pm\pm}$ in the diboson scenario, we have discussed the constraints at the past collider experiments. At the LEP experiment, by comparing the total decay width of the Z boson with the partial decay rate of $Z \to H^{++}H^{--}$, we have found that $m_{H^{\pm\pm}} < 42.9$ GeV is excluded at the 95% C.L. We also have calculated the number of events for various final states deduced from $e^+e^- \to H^{++}H^{--}$ at the LEP II. Although the signal with tetraleptons plus missing momentum cannot be used to derive a constraint on $m_{H^{\pm\pm}}$, due to the reduction of the signal cross section by a square of the branching fraction of $H^{\pm\pm} \to \ell^{\pm}\ell^{\pm}\nu\nu$ decay, the other signals which include a same-sign dilepton can be useful for the search for $H^{\pm\pm}$ in the diboson decay scenario. We have finished our discussion by emphasizing a need of dedicated analysis for these signals by using the data from the LEP II experiment.

We then have discussed the searches for $H^{\pm\pm}$ in the diboson decay scenario at the LHC and also have discussed the bound on the mass of $H^{\pm\pm}$ from the current data. In order to find evidence of $H^{\pm\pm}$ in relatively lower mass

[4] An effective $S^{\pm\pm}W^{\mp}W^{\mp}$ vertex for the singlet scalar boson $S^{\pm\pm}$ was recently discussed in Ref. [63].

TABLE IV. The same as Table III, but for the LHC with $\sqrt{s} = 8$ TeV.

LHC $\sqrt{s} = 8$ TeV, NLO with CT10 PDFs						
Mass [GeV]	$\sigma(H^{++}H^{--})$ [pb]		$\sigma(H^{++}H^{-})$ [pb]		$\sigma(H^{+}H^{--})$ [pb]	
50	8.52×10^{0}	$^{+2.0\%}_{-1.1\%}$ $^{+3.1\%}_{-3.5\%}$	1.06×10^{1}	$^{+2.0\%}_{-1.0\%}$ $^{+3.7\%}_{-4.3\%}$	6.71×10^{0}	$^{+2.2\%}_{-1.0\%}$ $^{+3.5\%}_{-4.1\%}$
60	3.57×10^{0}	$^{+1.4\%}_{-0.6\%}$ $^{+3.3\%}_{-3.4\%}$	4.47×10^{0}	$^{+1.3\%}_{-0.5\%}$ $^{+3.8\%}_{-4.4\%}$	2.73×10^{0}	$^{+1.5\%}_{-0.5\%}$ $^{+3.7\%}_{-4.1\%}$
70	1.93×10^{0}	$^{+1.0\%}_{-0.2\%}$ $^{+3.3\%}_{-3.6\%}$	2.36×10^{0}	$^{+0.9\%}_{-0.2\%}$ $^{+3.9\%}_{-4.5\%}$	1.40×10^{0}	$^{+1.0\%}_{-0.3\%}$ $^{+3.8\%}_{-4.3\%}$
80	1.16×10^{0}	$^{+0.6\%}_{-0.1\%}$ $^{+3.4\%}_{-3.7\%}$	1.40×10^{0}	$^{+0.5\%}_{-0.1\%}$ $^{+3.9\%}_{-4.7\%}$	8.03×10^{-1}	$^{+0.6\%}_{-0.1\%}$ $^{+3.9\%}_{-4.5\%}$
90	7.44×10^{-1}	$^{+0.6\%}_{-0.0\%}$ $^{+3.4\%}_{-3.9\%}$	8.91×10^{-1}	$^{+0.3\%}_{-0.0\%}$ $^{+4.0\%}_{-4.8\%}$	4.98×10^{-1}	$^{+0.3\%}_{-0.0\%}$ $^{+4.1\%}_{-4.7\%}$
100	5.01×10^{-1}	$^{+0.5\%}_{-0.1\%}$ $^{+3.5\%}_{-4.0\%}$	5.98×10^{-1}	$^{+0.5\%}_{-0.2\%}$ $^{+4.0\%}_{-5.0\%}$	3.26×10^{-1}	$^{+0.5\%}_{-0.1\%}$ $^{+4.3\%}_{-4.9\%}$
120	2.52×10^{-1}	$^{+0.8\%}_{-0.6\%}$ $^{+3.6\%}_{-4.5\%}$	3.01×10^{-1}	$^{+0.8\%}_{-0.7\%}$ $^{+4.2\%}_{-5.5\%}$	1.57×10^{-1}	$^{+0.8\%}_{-0.6\%}$ $^{+4.6\%}_{-5.3\%}$
140	1.39×10^{-1}	$^{+1.1\%}_{-1.0\%}$ $^{+3.8\%}_{-4.8\%}$	1.68×10^{-1}	$^{+1.1\%}_{-1.2\%}$ $^{+4.4\%}_{-5.8\%}$	8.37×10^{-2}	$^{+1.1\%}_{-1.1\%}$ $^{+4.9\%}_{-5.7\%}$
160	8.25×10^{-2}	$^{+1.3\%}_{-1.5\%}$ $^{+4.0\%}_{-5.0\%}$	1.00×10^{-1}	$^{+1.3\%}_{-1.5\%}$ $^{+4.7\%}_{-6.2\%}$	4.81×10^{-2}	$^{+1.4\%}_{-1.5\%}$ $^{+5.3\%}_{-6.1\%}$
180	5.14×10^{-2}	$^{+1.5\%}_{-1.8\%}$ $^{+4.2\%}_{-5.4\%}$	6.30×10^{-2}	$^{+1.5\%}_{-1.9\%}$ $^{+4.8\%}_{-6.7\%}$	2.92×10^{-2}	$^{+1.6\%}_{-1.9\%}$ $^{+5.6\%}_{-6.5\%}$
200	3.34×10^{-2}	$^{+1.7\%}_{-2.2\%}$ $^{+4.5\%}_{-5.7\%}$	4.13×10^{-2}	$^{+1.7\%}_{-2.2\%}$ $^{+5.1\%}_{-7.0\%}$	1.85×10^{-2}	$^{+1.8\%}_{-2.2\%}$ $^{+6.0\%}_{-7.0\%}$
250	1.28×10^{-2}	$^{+2.2\%}_{-2.9\%}$ $^{+5.1\%}_{-6.4\%}$	1.63×10^{-2}	$^{+2.2\%}_{-2.9\%}$ $^{+5.9\%}_{-8.1\%}$	6.81×10^{-3}	$^{+2.3\%}_{-3.0\%}$ $^{+7.0\%}_{-7.8\%}$
300	5.62×10^{-3}	$^{+2.6\%}_{-3.5\%}$ $^{+5.8\%}_{-7.1\%}$	7.30×10^{-3}	$^{+2.6\%}_{-3.6\%}$ $^{+6.8\%}_{-9.2\%}$	2.87×10^{-3}	$^{+2.7\%}_{-3.6\%}$ $^{+7.9\%}_{-8.8\%}$
350	2.68×10^{-3}	$^{+3.0\%}_{-4.1\%}$ $^{+6.4\%}_{-7.8\%}$	3.56×10^{-3}	$^{+3.0\%}_{-4.2\%}$ $^{+7.8\%}_{-10.4\%}$	1.32×10^{-3}	$^{+3.1\%}_{-4.2\%}$ $^{+9.1\%}_{-9.7\%}$
400	1.37×10^{-3}	$^{+3.4\%}_{-4.6\%}$ $^{+7.2\%}_{-8.5\%}$	1.84×10^{-3}	$^{+3.5\%}_{-4.7\%}$ $^{+9.0\%}_{-11.6\%}$	6.55×10^{-4}	$^{+3.5\%}_{-4.7\%}$ $^{+10.2\%}_{-10.7\%}$

TABLE V. The same as Table III, but for the LHC with $\sqrt{s} = 13$ TeV.

LHC $\sqrt{s} = 13$ TeV, NLO with CT10 PDFs						
Mass [GeV]	$\sigma(H^{++}H^{--})$ [pb]		$\sigma(H^{++}H^{-})$ [pb]		$\sigma(H^{+}H^{--})$ [pb]	
80	2.26×10^{0}	$^{+1.7\%}_{-0.8\%}$ $^{+3.0\%}_{-3.4\%}$	2.62×10^{0}	$^{+1.6\%}_{-0.7\%}$ $^{+3.5\%}_{-4.1\%}$	1.65×10^{0}	$^{+1.7\%}_{-0.7\%}$ $^{+3.4\%}_{-3.9\%}$
90	1.48×10^{0}	$^{+1.4\%}_{-0.5\%}$ $^{+3.1\%}_{-3.4\%}$	1.70×10^{0}	$^{+1.2\%}_{-0.5\%}$ $^{+3.7\%}_{-4.1\%}$	1.05×10^{0}	$^{+1.4\%}_{-0.5\%}$ $^{+3.5\%}_{-3.9\%}$
100	1.02×10^{0}	$^{+1.1\%}_{-0.3\%}$ $^{+3.1\%}_{-3.5\%}$	1.16×10^{0}	$^{+1.0\%}_{-0.3\%}$ $^{+3.7\%}_{-4.2\%}$	7.02×10^{-1}	$^{+1.1\%}_{-0.3\%}$ $^{+3.6\%}_{-4.0\%}$
120	5.33×10^{-1}	$^{+0.6\%}_{-0.1\%}$ $^{+3.2\%}_{-3.6\%}$	6.07×10^{-1}	$^{+0.5\%}_{-0.1\%}$ $^{+3.7\%}_{-4.4\%}$	3.53×10^{-1}	$^{+0.6\%}_{-0.1\%}$ $^{+3.8\%}_{-4.2\%}$
140	3.07×10^{-1}	$^{+0.4\%}_{-0.0\%}$ $^{+3.2\%}_{-3.8\%}$	3.50×10^{-1}	$^{+0.3\%}_{-0.0\%}$ $^{+3.8\%}_{-4.6\%}$	1.97×10^{-1}	$^{+0.3\%}_{-0.0\%}$ $^{+3.9\%}_{-4.5\%}$
160	1.89×10^{-1}	$^{+0.5\%}_{-0.2\%}$ $^{+3.4\%}_{-3.9\%}$	2.17×10^{-1}	$^{+0.5\%}_{-0.2\%}$ $^{+4.0\%}_{-4.8\%}$	1.18×10^{-1}	$^{+0.5\%}_{-0.2\%}$ $^{+4.2\%}_{-4.7\%}$
180	1.22×10^{-1}	$^{+0.7\%}_{-0.4\%}$ $^{+3.5\%}_{-4.1\%}$	1.41×10^{-1}	$^{+0.7\%}_{-0.5\%}$ $^{+4.1\%}_{-5.1\%}$	7.48×10^{-2}	$^{+0.7\%}_{-0.5\%}$ $^{+4.3\%}_{-5.0\%}$
200	8.23×10^{-2}	$^{+0.8\%}_{-0.7\%}$ $^{+3.5\%}_{-4.3\%}$	9.58×10^{-2}	$^{+0.8\%}_{-0.8\%}$ $^{+4.2\%}_{-5.3\%}$	4.95×10^{-2}	$^{+0.8\%}_{-0.8\%}$ $^{+4.6\%}_{-5.2\%}$
250	3.48×10^{-2}	$^{+1.2\%}_{-1.4\%}$ $^{+3.8\%}_{-4.9\%}$	4.14×10^{-2}	$^{+1.2\%}_{-1.4\%}$ $^{+4.5\%}_{-6.0\%}$	2.01×10^{-2}	$^{+1.2\%}_{-1.4\%}$ $^{+5.1\%}_{-5.9\%}$
300	1.68×10^{-2}	$^{+1.5\%}_{-1.9\%}$ $^{+4.2\%}_{-5.4\%}$	2.03×10^{-2}	$^{+1.5\%}_{-1.9\%}$ $^{+4.9\%}_{-6.6\%}$	9.34×10^{-3}	$^{+1.6\%}_{-2.0\%}$ $^{+5.6\%}_{-6.6\%}$
350	8.82×10^{-3}	$^{+1.8\%}_{-2.3\%}$ $^{+4.6\%}_{-5.8\%}$	1.09×10^{-2}	$^{+1.8\%}_{-2.4\%}$ $^{+5.2\%}_{-7.3\%}$	4.77×10^{-3}	$^{+1.9\%}_{-2.4\%}$ $^{+6.2\%}_{-7.2\%}$
400	4.95×10^{-3}	$^{+2.0\%}_{-2.8\%}$ $^{+5.0\%}_{-6.2\%}$	6.22×10^{-3}	$^{+2.0\%}_{-2.8\%}$ $^{+5.8\%}_{-7.9\%}$	2.61×10^{-3}	$^{+2.1\%}_{-2.9\%}$ $^{+6.8\%}_{-7.7\%}$
450	2.92×10^{-3}	$^{+2.3\%}_{-3.1\%}$ $^{+5.3\%}_{-6.8\%}$	3.72×10^{-3}	$^{+2.3\%}_{-3.1\%}$ $^{+6.4\%}_{-8.6\%}$	1.50×10^{-3}	$^{+2.4\%}_{-3.2\%}$ $^{+7.5\%}_{-8.3\%}$
500	1.79×10^{-3}	$^{+2.5\%}_{-3.4\%}$ $^{+5.7\%}_{-7.2\%}$	2.31×10^{-3}	$^{+2.5\%}_{-3.5\%}$ $^{+6.9\%}_{-9.3\%}$	9.00×10^{-4}	$^{+2.6\%}_{-3.6\%}$ $^{+8.1\%}_{-8.9\%}$
550	1.13×10^{-3}	$^{+2.7\%}_{-3.8\%}$ $^{+6.2\%}_{-7.6\%}$	1.48×10^{-3}	$^{+2.8\%}_{-3.8\%}$ $^{+7.6\%}_{-10.1\%}$	5.58×10^{-4}	$^{+2.9\%}_{-3.9\%}$ $^{+8.8\%}_{-9.4\%}$

regions, we treat the theoretical framework for the inclusive same-sign dilepton signal, which consists of total cross sections for $H^{\pm\pm}$ production at the NLO, the decay branching ratio into the same-flavor dilepton decay with interference effects, and efficiencies for detector acceptance and the kinematical cuts. By combining them, we have evaluated the theoretical prediction for the fiducial cross section for the same-sign dimuon events. By comparing it with the upper limit reported by the ATLAS Collaboration using the 4.7 fb^{-1} data at the 7 TeV run, we find that the

TABLE VI. The same as Table III, but for the LHC with $\sqrt{s} = 14$ TeV.

LHC $\sqrt{s} = 14$ TeV, NLO with CT10 PDFs						
Mass [GeV]	$\sigma(H^{++}H^{--})$ [pb]		$\sigma(H^{++}H^{-})$ [pb]		$\sigma(H^{+}H^{--})$ [pb]	
80	2.49×10^{0}	$^{+1.8\%\ +3.0\%}_{-0.9\%\ -3.4\%}$	2.87×10^{0}	$^{+1.7\%\ +3.4\%}_{-0.9\%\ -4.1\%}$	1.83×10^{0}	$^{+1.9\%\ +3.3\%}_{-0.9\%\ -3.8\%}$
90	1.64×10^{0}	$^{+1.5\%\ +3.1\%}_{-0.7\%\ -3.3\%}$	1.87×10^{0}	$^{+1.4\%\ +3.6\%}_{-0.6\%\ -4.0\%}$	1.17×10^{0}	$^{+1.6\%\ +3.5\%}_{-0.6\%\ -3.8\%}$
100	1.13×10^{0}	$^{+1.2\%\ +3.1\%}_{-0.5\%\ -3.3\%}$	1.28×10^{0}	$^{+1.1\%\ +3.5\%}_{-0.4\%\ -4.2\%}$	7.84×10^{-1}	$^{+1.3\%\ +3.6\%}_{-0.5\%\ -3.8\%}$
120	5.93×10^{-1}	$^{+0.8\%\ +3.1\%}_{-0.2\%\ -3.5\%}$	6.71×10^{-1}	$^{+0.7\%\ +3.7\%}_{-0.1\%\ -4.3\%}$	3.96×10^{-1}	$^{+0.8\%\ +3.7\%}_{-0.2\%\ -4.1\%}$
140	3.43×10^{-1}	$^{+0.4\%\ +3.2\%}_{-0.0\%\ -3.7\%}$	3.89×10^{-1}	$^{+0.3\%\ +3.8\%}_{-0.0\%\ -4.5\%}$	2.22×10^{-1}	$^{+0.3\%\ +3.9\%}_{-0.0\%\ -4.3\%}$
160	2.12×10^{-1}	$^{+0.4\%\ +3.3\%}_{-0.0\%\ -3.8\%}$	2.41×10^{-1}	$^{+0.5\%\ +3.7\%}_{-0.1\%\ -4.8\%}$	1.34×10^{-1}	$^{+0.4\%\ +4.2\%}_{-0.0\%\ -4.5\%}$
180	1.38×10^{-1}	$^{+0.5\%\ +3.4\%}_{-0.3\%\ -4.0\%}$	1.58×10^{-1}	$^{+0.6\%\ +3.9\%}_{-0.4\%\ -5.0\%}$	8.53×10^{-2}	$^{+0.5\%\ +4.3\%}_{-0.3\%\ -4.7\%}$
200	9.33×10^{-2}	$^{+0.7\%\ +3.4\%}_{-0.5\%\ -4.2\%}$	1.08×10^{-1}	$^{+0.7\%\ +4.0\%}_{-0.6\%\ -5.2\%}$	5.67×10^{-2}	$^{+0.7\%\ +4.4\%}_{-0.6\%\ -5.0\%}$
250	3.99×10^{-2}	$^{+1.1\%\ +3.8\%}_{-1.1\%\ -4.6\%}$	4.70×10^{-2}	$^{+1.0\%\ +4.3\%}_{-1.2\%\ -5.8\%}$	2.33×10^{-2}	$^{+1.1\%\ +4.9\%}_{-1.2\%\ -5.7\%}$
300	1.94×10^{-2}	$^{+1.4\%\ +4.0\%}_{-1.7\%\ -5.1\%}$	2.33×10^{-2}	$^{+1.4\%\ +4.7\%}_{-1.7\%\ -6.3\%}$	1.10×10^{-2}	$^{+2.5\%\ +5.4\%}_{-1.7\%\ -6.3\%}$
350	1.03×10^{-2}	$^{+1.6\%\ +4.3\%}_{-2.1\%\ -5.6\%}$	1.26×10^{-2}	$^{+1.6\%\ +5.1\%}_{-2.2\%\ -6.9\%}$	5.66×10^{-3}	$^{+1.7\%\ +5.9\%}_{-2.2\%\ -6.9\%}$
400	5.85×10^{-3}	$^{+1.9\%\ +4.7\%}_{-2.5\%\ -6.0\%}$	7.28×10^{-3}	$^{+1.9\%\ +5.5\%}_{-2.5\%\ -7.5\%}$	3.13×10^{-3}	$^{+2.0\%\ +6.5\%}_{-2.6\%\ -7.4\%}$
450	3.49×10^{-3}	$^{+2.1\%\ +5.1\%}_{-2.8\%\ -6.4\%}$	4.41×10^{-3}	$^{+2.1\%\ +6.0\%}_{-2.9\%\ -8.2\%}$	1.82×10^{-3}	$^{+2.2\%\ +7.1\%}_{-2.9\%\ -7.9\%}$
500	2.16×10^{-3}	$^{+2.3\%\ +5.5\%}_{-3.2\%\ -6.8\%}$	2.77×10^{-3}	$^{+2.3\%\ +6.5\%}_{-3.2\%\ -8.8\%}$	1.10×10^{-3}	$^{+2.5\%\ +7.6\%}_{-3.3\%\ -8.5\%}$
550	1.38×10^{-3}	$^{+2.6\%\ +5.8\%}_{-3.5\%\ -7.3\%}$	1.79×10^{-3}	$^{+2.6\%\ +7.1\%}_{-3.6\%\ -9.5\%}$	6.93×10^{-4}	$^{+2.7\%\ +8.2\%}_{-3.6\%\ -9.0\%}$

lower limit of $m_{H^{\pm\pm}}$ in the diboson decay scenario is revised to 60–68 GeV depending on the estimation of the signal efficiency in the search. We have estimated by naive extrapolation that the limit can be extended up to 85–90 GeV, if full analysis with the available 20 fb^{-1} data set at the 8 TeV run is performed.

Our analysis shows that relatively light $H^{\pm\pm}$ with $m_{H^{\pm\pm}} \simeq 100$ GeV are still allowed if $H^{\pm\pm}$ dominantly decay into (off-shell) dibosons. In the near future at the LHC run with 13–14 TeV, the searches for $H^{\pm\pm}$ in the diboson decay scenario will be performed to push the limit toward a few hundred GeV [30,36]. At the future lepton colliders, such as the ILC [58] and CLIC [59,60], we also have a chance to study the properties of not only $H^{\pm\pm}$ but also the other tripletlike Higgs bosons [61] as long as the masses of them are within the reach of these colliders.

ACKNOWLEDGMENTS

We thank Koji Terashi for useful discussions. This work was supported in part by Grant-in-Aid for Scientific Research, No. 22244031, No. 23104006, and No. 24340046, JSPS, No. 25·10031, and the National Science Council of Republic of China under Grant No. NSC-101-2811-M-008-014.

APPENDIX: $H^{\pm\pm}$ PRODUCTION CROSS SECTIONS AT THE LHC

In this Appendix, we present the cross sections for $H^{\pm\pm}$ production at the LHC. We consider the three processes $pp \to H^{++}H^{--}$, $H^{++}H^{-}$, and $H^{+}H^{--}$ at the LHC with $\sqrt{s} = 7$, 8, 13, and 14 TeV. We evaluate the total cross sections at the NLO in QCD [48] with CT10 PDFs [64] and also their uncertainties by taking into account the scale ambiguity and the PDF uncertainty. For the latter two processes, the mass of $H^{\pm}$ is taken to be $m_{H^{\pm}} = m_{H^{\pm\pm}}$ for simplicity.

The scale ambiguity is estimated by seeking the maximum and minimum cross sections by varying the factorization and renormalization scales $\mu = \mu_F = \mu_R$ in the range $Q^2/10 < \mu < 10Q^2$, where Q is the invariant mass of the final-state scalar pair. The PDF uncertainties are calculated according to the Hessian method with 26 eigenvector set provided in Ref. [64].

In Table III, the total cross section at the NLO with $\mu = Q$, its uncertainties from the scale choice, and the PDF, in order, are presented for the three processes for various values of $m_{H^{\pm\pm}}$ at the LHC with $\sqrt{s} = 7$ TeV. The same results but for $\sqrt{s} = 8$, 13, and 14 TeV are also presented in Tables IV, V, and VI, respectively.

[1] ATLAS Collaboration, Phys. Lett. B **716**, 1 (2012); CMS Collaboration, Phys. Lett. B **716**, 30 (2012).

[2] ATLAS Collaboration, Report No. ATLAS-CONF-2013-034; CMS Collaboration, Report No. CMS-PAS-HIG-12-045.

[3] ATLAS Collaboration, Phys. Lett. B **726**, 88 (2013); **726**, 120 (2013); CMS Collaboration, J. High Energy Phys. 01 (2014) 096; Phys. Rev. D **89**, 092007 (2014).

[4] S. Weinberg, Phys. Rev. Lett. **37**, 657 (1976); J. Liu and L. Wolfenstein, Nucl. Phys. **B289**, 1 (1987).

[5] K. Funakubo, A. Kakuto, and K. Takenaga, Prog. Theor. Phys. **91**, 341 (1994); A. T. Davies, C. D. Froggatt, G. Jenkins, and R. G. Moorhouse, Phys. Lett. B **336**, 464 (1994); J. M. Cline, K. Kainulainen, and A. P. Vischer, Phys. Rev. D **54**, 2451 (1996); L. Fromme, S. J. Huber, and M. Seniuch, J. High Energy Phys. 11 (2006) 038.

[6] A. I. Bochkarev, S. V. Kuzmin, and M. E. Shaposhnikov, Phys. Lett. B **244**, 275 (1990); A. E. Nelson, D. B. Kaplan, and A. G. Cohen, Nucl. Phys. **B373**, 453 (1992); N. Turok and J. Zadrozny, Nucl. Phys. **B369**, 729 (1992).

[7] S. Khalil, J. Phys. G **35**, 055001 (2008); S. Iso, N. Okada, and Y. Orikasa, Phys. Lett. B **676**, 81 (2009); Phys. Rev. D **80**, 115007 (2009).

[8] T. P. Cheng and L. F. Li, Phys. Rev. D **22**, 2860 (1980); J. Schechter and J. W. F. Valle, Phys. Rev. D **22**, 2227 (1980); G. Lazarides, Q. Shafi, and C. Wetterich, Nucl. Phys. **B181**, 287 (1981); R. N. Mohapatra and G. Senjanovic, Phys. Rev. D **23**, 165 (1981); M. Magg and C. Wetterich, Phys. Lett. B **94**, 61 (1980).

[9] A. Zee, Phys. Lett. **93B**, 389 (1980); **95B**, 461(E) (1980); **161B**, 141 (1985); Nucl. Phys. **B264**, 99 (1986); K. S. Babu, Phys. Lett. B **203**, 132 (1988).

[10] L. M. Krauss, S. Nasri, and M. Trodden, Phys. Rev. D **67**, 085002 (2003); K. Cheung and O. Seto, Phys. Rev. D **69**, 113009 (2004).

[11] E. Ma, Phys. Rev. D **73**, 077301 (2006); Phys. Lett. B **717**, 235 (2012); J. Kubo, E. Ma, and D. Suematsu, Phys. Lett. B **642**, 18 (2006); D. Schmidt, T. Schwetz, and T. Toma, Phys. Rev. D **85**, 073009 (2012).

[12] M. Aoki, S. Kanemura, and O. Seto, Phys. Rev. Lett. **102**, 051805 (2009); Phys. Rev. D **80**, 033007 (2009); M. Aoki, S. Kanemura, and K. Yagyu, Phys. Rev. D **83**, 075016 (2011).

[13] N. G. Deshpande and E. Ma, Phys. Rev. D **18**, 2574 (1978); R. Barbieri, L. J. Hall, and V. S. Rychkov, Phys. Rev. D **74**, 015007 (2006).

[14] J. McDonald, Phys. Rev. D **50**, 3637 (1994); C. P. Burgess, M. Pospelov, and T. ter Veldhuis, Nucl. Phys. **B619**, 709 (2001).

[15] J. F. Gunion, C. Loomis, and K. T. Pitts, arXiv:hep-ph/9610237; K. Huitu, J. Maalampi, A. Pietila, and M. Raidal, Nucl. Phys. **B487**, 27 (1997).

[16] S. Chakrabarti, D. Choudhury, R. M. Godbole, and B. Mukhopadhyaya, Phys. Lett. B **434**, 347 (1998).

[17] E. J. Chun, K. Y. Lee, and S. C. Park, Phys. Lett. B **566**, 142 (2003).

[18] G. Azuelos *et al.*, Eur. Phys. J. C **39S2**, 13 (2005); G. Azuelos, K. Benslama, and J. Ferland, J. Phys. G **32**, 73 (2006).

[19] A. G. Akeroyd and M. Aoki, Phys. Rev. D **72**, 035011 (2005).

[20] A. Hektor, M. Kadastik, M. Muntel, M. Raidal, and L. Rebane, Nucl. Phys. **B787**, 198 (2007); J. Garayoa and T. Schwetz, J. High Energy Phys. 03 (2008) 009; M. Kadastik, M. Raidal, and L. Rebane, Phys. Rev. D **77**, 115023 (2008); A. G. Akeroyd, M. Aoki, and H. Sugiyama, Phys. Rev. D **77**, 075010 (2008).

[21] T. Han, B. Mukhopadhyaya, Z. Si, and K. Wang, Phys. Rev. D **76**, 075013 (2007).

[22] P. Fileviez Perez, T. Han, G.-y. Huang, T. Li, and K. Wang, Phys. Rev. D **78**, 015018 (2008).

[23] F. del Águila and J. A. Aguilar-Saavedra, Nucl. Phys. **B813**, 22 (2009); A. G. Akeroyd and C.-W. Chiang, Phys. Rev. D **80**, 113010 (2009); A. G. Akeroyd, C. W. Chiang, and N. Gaur, J. High Energy Phys. 11 (2010) 005.

[24] S. Godfrey and K. Moats, Phys. Rev. D **81**, 075026 (2010).

[25] A. G. Akeroyd and C.-W. Chiang, Phys. Rev. D **81**, 115007 (2010).

[26] A. G. Akeroyd and H. Sugiyama, Phys. Rev. D **84**, 035010 (2011).

[27] A. Melfo, M. Nemevsek, F. Nesti, G. Senjanovic, and Y. Zhang, Phys. Rev. D **85**, 055018 (2012).

[28] M. Aoki, S. Kanemura, and K. Yagyu, Phys. Rev. D **85**, 055007 (2012).

[29] A. G. Akeroyd, S. Moretti, and H. Sugiyama, Phys. Rev. D **85**, 055026 (2012).

[30] C.-W. Chiang, T. Nomura, and K. Tsumura, Phys. Rev. D **85**, 095023 (2012).

[31] E. J. Chun and P. Sharma, J. High Energy Phys. 08 (2012) 162; Phys. Lett. B **728**, 256 (2014).

[32] H. Sugiyama, K. Tsumura, and H. Yokoya, Phys. Lett. B **717**, 229 (2012).

[33] S. Kanemura, K. Yagyu, and H. Yokoya, Phys. Lett. B **726**, 316 (2013).

[34] F. del Águila and M. Chala, J. High Energy Phys. 03 (2014) 027.

[35] B. Dutta, R. Eusebi, Y. Gao, T. Ghosh, and T. Kamon, Phys. Rev. D **90**, 055015 (2014).

[36] Z. Kang, J. Li, T. Li, Y. Liu, and G.-Z. Ning, arXiv:1404.5207.

[37] M. Aoki, S. Kanemura, M. Kikuchi, and K. Yagyu, Phys. Rev. D **87**, 015012 (2013).

[38] A. G. Akeroyd, S. Moretti, and H. Sugiyama, Phys. Lett. B **728**, 157 (2014).

[39] J. Abdallah *et al.* (DELPHI Collaboration), Phys. Lett. B **552**, 127 (2003); P. Achard *et al.* (L3 Collaboration), Phys. Lett. B **576**, 18 (2003); G. Abbiendi *et al.* (OPAL Collaboration), Phys. Lett. B **526**, 221 (2002).

[40] A. Aktas *et al.* (H1 Collaboration), Phys. Lett. B **638**, 432 (2006).

[41] D. Acosta *et al.* (CDF Collaboration), Phys. Rev. Lett. **93**, 221802 (2004); **95**, 071801 (2005); T. Aaltonen *et al.* (CDF Collaboration), Phys. Rev. Lett. **101**, 121801 (2008).

[42] V. M. Abazov *et al.* (D0 Collaboration), Phys. Rev. Lett. **93**, 141801 (2004); **101**, 071803 (2008); **108**, 021801 (2012).

[43] ATLAS Collaboration, Eur. Phys. J. C **72**, 2244 (2012).

[44] CMS Collaboration, Eur. Phys. J. C **72**, 2189 (2012).

[45] ATLAS Collaboration, J. High Energy Phys. 12 (2012) 007.

[46] P. Dey, A. Kundu, and B. Mukhopadhyaya, J. Phys. G **36**, 025002 (2009).
[47] J. Beringer *et al.*, Phys. Rev. D **86**, 010001 (2012).
[48] M. Muhlleitner and M. Spira, Phys. Rev. D **68**, 117701 (2003).
[49] J. Pumplin, D. R. Stump, J. Huston, H-L. Lai, P. Nadolsky, and Wu-Ki Tung, J. High Energy Phys. 07 (2002) 012.
[50] S. Schael *et al.* (ALEPH and DELPHI and L3 and OPAL and SLD and LEP Electroweak Working Group and SLD Electroweak Group and SLD Heavy Flavour Group Collaborations), Phys. Rep. **427**, 257 (2006).
[51] S. Schael *et al.* (ALEPH and DELPHI and L3 and OPAL and LEP Electroweak Collaborations), Phys. Rep. **532**, 119 (2013).
[52] P. Achard *et al.* (L3 Collaboration), Phys. Lett. B **600**, 22 (2004).
[53] G. Abbiendi *et al.* (OPAL Collaboration), Phys. Lett. B **440**, 393 (1998).
[54] G. Abbiendi *et al.* (OPAL Collaboration), Eur. Phys. J. C **40**, 287 (2005).
[55] M. Herquet, F. Maltoni, O. Mattelaer, and T. Stelzer, J. High Energy Phys. 06 (2011) 128.
[56] B. K. Bullock, K. Hagiwara, and A. D. Martin, Nucl. Phys. **B395**, 499 (1993).
[57] S. Kawabata, Y. Shimizu, Y. Sumino, and H. Yokoya, Phys. Lett. B **710**, 658 (2012); J. High Energy Phys. 08 (2013) 129.
[58] H. Baer *et al.*, arXiv:1306.6352.
[59] E. Accomando *et al.* (CLIC Physics Working Group Collaboration), arXiv:hep-ph/0412251.
[60] L. Linssen, A. Miyamoto, M. Stanitzki, and H. Weerts, arXiv:1202.5940.
[61] K. Yagyu, arXiv:1405.5149.
[62] J. Cao and J.-F. Shen, Mod. Phys. Lett. A **29**, 1450041 (2014).
[63] S. F. King, A. Merle, and L. Panizzi, arXiv:1406.4137 [J. High Energy Phys. (to be published)].
[64] H.-L. Lai, M. Guzzi, J. Huston, Z. Li, P. M. Nadolsky, J. Pumplin, and C.-P. Yuan, Phys. Rev. D **82**, 074024 (2010).